Spatio-Temporal Binding and Dynamic Cortical Organization: Research Issues

Richard B. Wells

March, 2005

I. Abstract

What is the nature of the cortical organization that gives rise to binding codes in the neural representation of objects and events? Unfortunately, the details of cortical circuit connection and many of the details of cortical cell physiology are far from completely understood. Furthermore, none of the current hypothetical structures proposed by various researchers are free from disagreement with experimental data at the detail level. In this paper those facts that are generally agreed to at the present time by a majority of neuroscientists are reviewed with the goal of putting together a comprehensive picture of the role of functional column structure in the neocortex. We first review the state of knowledge of neocortical organization. We then review the mathematical theories of oscillator and wave models in the context of functional column structure and discuss their implications for larger-scale modeling of object and event binding through retroactive multiregional feedback. In the course of this review, we will examine the implications for the chain-of-oscillators, synchrony, and wave propagation paradigms for modeling neural binding code mechanisms.

II. Organization of Cortical Layers

It is well known that the neocortex has a layered structure with three superficial layers (layers I-III) and three deep layers (IV-VI). The cortex thickness ranges from about 2 mm to about 4 mm. Functional columns are believed to extend through the entire depth of the cortex and to be a fraction of a mm in diameter. Layer organization shows the following general tendencies [1]:

- Layer I is called the acellular layer and contains dendrites from deeper-lying neurons and axons that travel and form connections in this layer. It contains very few neurons [2], and those it does contain are inhibitory interneurons [11].
- Layer II is comprised mostly of granular cells and apical dendrites from neurons in layers V and VI. Kelly [2] tells us that layer II cells are primarily small pyramidal cells, and that layers II and III supply much of the output to other cortical regions.
- Layer III contains a variety of cells, most of which are small pyramidal cells.
- Layer IV is also composed of granular cells. White [3] tells us that these are local plexus, basket, and chandelier cells, all of which are inhibitory interneurons. Spiny stellate cells are also found exclusively in layer IV.
- Layer V is comprised mostly of large pyramidal cells. It also contains basal dendrites of neurons in layers III and IV. White [3] tells us that at least the axons and possibly basal dendrites of non-spiny bipolar cells are found in layer V, as well as local plexus cells. There are two types of non-spiny bipolar cells, one of which is

inhibitory and the other of which appears to be excitatory. White also tells us that chandelier cells are found in layer V. Kelly [2] tells us that layer V contains the largest pyramidal cells, and that these cells project long axons that leave the cortex and descend to the basal ganglia, brain stem, and spinal cord.

- Layer VI is a heterogeneous layer of neurons blending into the white matter. It also contains basal dendrites from neurons in layers III and IV. Kelly [2] tells us that many layer VI pyramidal cells project back to the thalamus.

Most cortical neurons can be classified according to signaling properties into four groups: regular spiking (RS), fast spiking (FS), intrinsic bursting (IB), and continuously spiking (CS). Computational models for each of these types have been provided by Wilson [4]. Excitatory neurons in the superficial layers tend to be RS-type. The deeper layers contain excitatory neurons of both the RS- and IB- or CB- types. 50% of the inhibitory interneurons in the neocortex are the FS-type [5]. With regard to the bursting neurons, it is worth noting that in many cases bursting in neocortical neurons is not endogenous but rather is a condition that is evoked experimentally by means of injecting a constant-current stimulus into the cell [6, pp. 165-6].

III. Cortical Circuit Models

Various models of cortical circuit organization have been proposed over the years. As we review these models, one point to emphasize at the start is that many of the neuronal connections depicted are hypothetical. Generally, the determination of connectivity in the neocortex requires painstaking anatomical study. The experimental issues involved are described in [3].

One of the earlier models was proposed by Shepherd in 1978 [7]. Shepherd's model, reproduced from [8] along with his caption given there, is shown in figure 1. (Note that in this caption Shepherd's 1978 citation is misprinted as 1987). This model is now out-of-date and has been replaced by more accurate versions. Shepherd's model speculates that some pyramidal neurons in layers II and III feed their own output signals back into their own dendritic tree. This feedback pathway is generally not depicted in more recent models. Nonetheless, Shepherd's circuit contains some useful information often taken for granted in most of the more up-to-date models.

First, Shepherd proposes that neocortical organization follows a general framework exhibited elsewhere in the brain (in particular, in the olfactory cortex and the hippocampus). He calls this the olfactory-hippocampal-general cortex model. The 'simple cortex' (A in figure 1) is modeled after the olfactory cortex. The 'primary afferents' depicted in figure 1A are indeed sensory afferents in the olfactory cortex, but this is not the case for the general cortex where primary afferents come by way of the thalamus and mostly target neurons in layer IV. Afferents in layer I

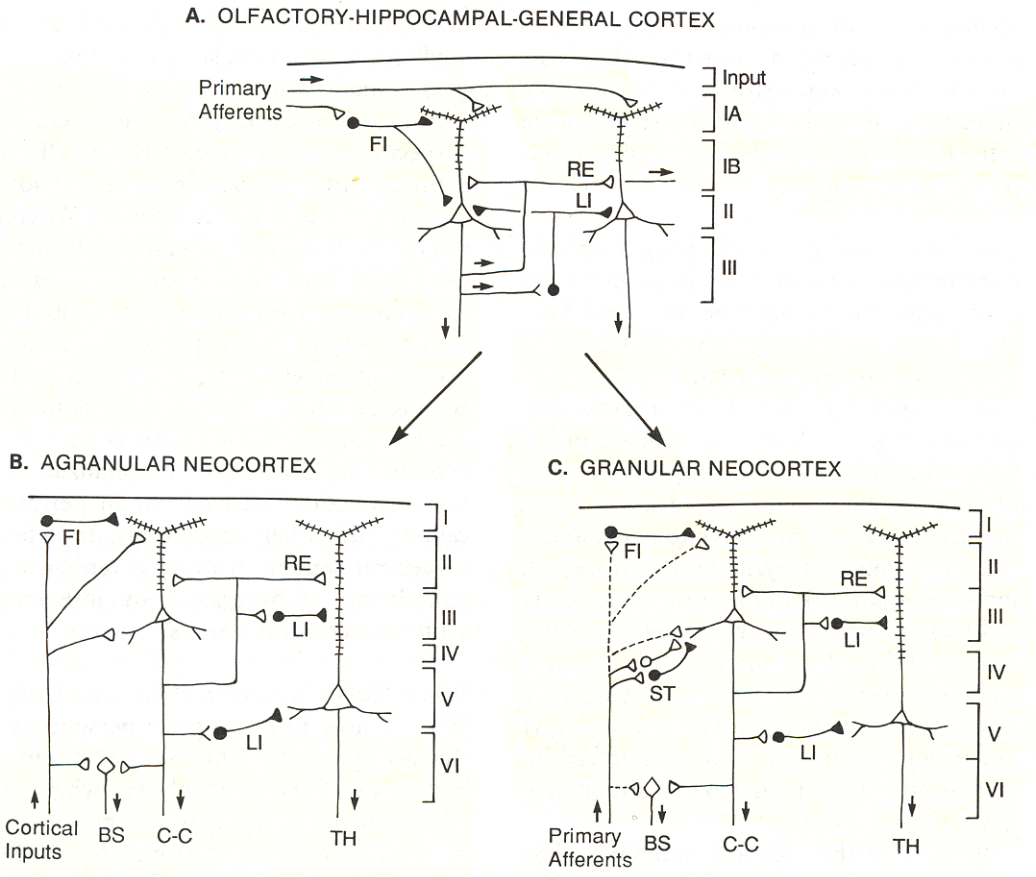

Fig. 30.9 Principles of local circuit organization in the cerebral cortex. **A.** Simple cortex, as represented by olfactory cortex, hippocampus, and reptilian dorsal (general) cortex. Layers indicated on right. FI, feedforward inhibition; LI, lateral (and feedback) inhibition; RE, recurrent (and lateral) excitation. **B.** Agranular motor and association areas of neocortex. Layers on right. Output sites below: BS, brainstem; C–C, corticocortical; TH, thalamus. **C.** Granular sensory and association areas of neocortex. Note that the main difference from the circuit in B is the predominance of primary afferents from the thalamus which project to an intracortical relay through stellate (ST) cells in layer IV. Connections to other layers are still present, but less prominent (dashed lines). Excitatory connections shown by open profiles; inhibitory, by closed profiles. (Modified from Shepherd, 1987)

Figure 1: Shepherd's model of cortical circuit organization. This model is now out of date.

are therefore primarily laterals from nearby cortical columns. These axons are generally unmyelinated (layer I is part of the 'gray matter') and, consequently, it may be presumed that their sources are within a few mm of the receiving column. Although layer I is called the acellular layer, it does contain sparse populations of neurogliaform cells (inhibitory interneurons (INs) that target dendritic shafts), inhibitory Cajal-Retzius, and "small layer I" cells that target dendrites and dendritic tufts. It is reasonable to posit that layer II/III pyramidal neurons make recurrent connections (RE in figure 1) with other layer II pyramidal neurons. However, self-looping feedback such as that depicted in figure 1A does not appear to be confirmed by later studies.

The agranular neocortex model (figure 1B) and the granular neocortex model (figure 1C) are in slightly better agreement with more recent models, although once again it is to be emphasized that in the primary sensory cortex it is the thalamus that is the principal pathway for sensory afferents in figure 1C. In the case of the association and motor cortices (1B), the cortical inputs are likely to be layer I collaterals from nearby functional columns and layer III projections from other columns (if they come in from the white matter). The latter is because the main projection neurons in the neocortex found in layer V project mainly to the basal ganglia, brain stem or spinal cord, while layer VI projection neurons project back to the thalamus [2]. Layer II pyramidal neurons project mainly to layer IV. Layer III projection neurons, on the other hand, appear to be the principal cortex-to-cortex projection neurons. Unmyelinated axon collaterals from these neurons most likely travel, via layer I, to nearby columns. The main trunks of their axons project to more distant columns via the white matter [2]. Therefore direct column-to-column signaling is to be attributed to layer III pyramidal cells, while any column-to-column signaling via layers V and VI pyramidal cells is going to be indirect. This is because these cells signal via pathways that can only return to the cortex via the thalamus. For instance, the basal ganglia signal to the prefrontal, premotor and motor cortices by projecting their outputs to the thalamus, and it is via the thalamus that these signals re-enter the cortex [9].

This organization is reflected in a more up-to-date model proposed by Douglas and Martin and depicted in figure 2. Figure 2 gives the impression of considerably more detail than Shepherd's model, but to a large degree this is illusory. First, figure 2 is greatly oversimplified inasmuch as it omits a great many intra-columnar interconnections and depicts only three types of cortical cells (pyramidal, spiny stellate, and smooth stellate). It also does not distinguish between spiny stellate cells and pyramidal cells. Third, the connections that are shown are putative rather than anatomically confirmed.

White [3] has ascertained some of the anatomically correct connections present in the neocortex, and this is depicted in figure 3. Again, it is to be understood that even figure 3 is some-what misleading inasmuch as the ratio of excitatory cells (pyramidal and spiny stellate) to inhibitory cells is not biologically correct. In the cortex only about 15% of the cells are inhibitory. Figure 3 puts the inhibitory neuron population much higher relative to the excitatory cell population.

It is often presumed that the ratio of inhibitory to excitatory synaptic connections follows the ratio of inhibitory to excitatory cell populations. However, this too is an assumption. Inhibitory INs make primarily local connections with perhaps a few inter-columnar connections made at the

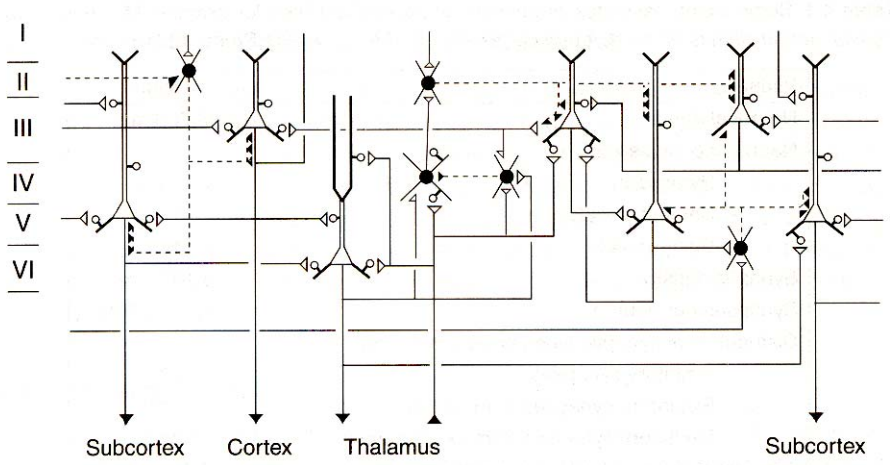

Fig. 4.4 Schematic connectivity patterns between neurons in a cortical layer. Open cell bodies represent (spiny) excitatory neurons such as the pyramidal neuron and the spiny stellate neuron. Their axons are plotted with solid lines that end at open triangles that represent the axon terminal. The dendritic boutons are indicated by open circles. Inhibitory (smooth) stellate neurons have solid cell bodies and synaptic terminal, and the axons are represented by dashed lines. [Adapted from Douglas and Martin, in *Synaptic organization of the brain*, Shepherd (ed.) (1990).]

Figure 2: The Douglas-Martin model. This figure is taken from [10], pg. 63.

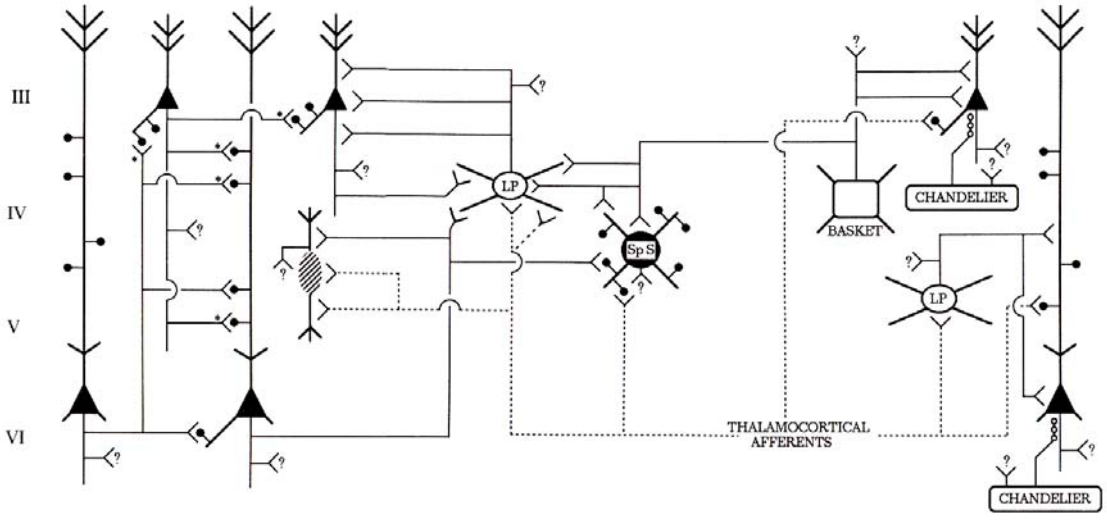

Figure 3.9. *Summary diagram illustrating the synaptic connections in cortex that have been conclusively demonstrated by labeling both their pre- and postsynaptic elements in single preparations. Also shown are several synapses (*) whose existence is highly likely (see the "Intrinsic Connections of Pyramidal Neurons" section). Neurons whose axons form asymmetrical synapses, that is pyramidal neurons and spiny stellate cells (SpS), are shown in solid black; neurons whose axons form symmetrical synapses, that is local plexus (LP), basket, and chandelier cells, are unfilled. The two varieties of nonspiny bipolar cells, one having an axon that forms asymmetrical synapses and the other an axon that forms symmetrical ones, are shown by a single crosshatched cell. Thalamocortical afferents are shown by dashed lines.*

Figure 3: Anatomically confirmed cortical connections**.** The figure is taken from [3].

boundaries between adjacent functional columns. (These 'boundary connections' are one posited mechanism for the hypothesis that functional columns are non-static structures and can dynamically re-arrange their organization [3]). White and his collaborators have proposed several

general rules of cortical organization. They are [3]:

- Rule 1. Every neuron within the target area of a projection receives input from the projection.

- Corollary to Rule 1. Axon terminals from any extrinsic or intrinsic source synapse onto every morphological or physiological neuron type within their terminal projection field. In practice this means that a pathway will form synapses with every element in their target region capable of forming the type of synapse normally made by the pathway, i.e., asymmetrical (excitatory) or symmetrical (inhibitory).

- Rule 2. Different dendrites of a single neuron form similar synaptic patterns; that is, the numbers, types proportions, and spatial distribution of synapses is similar, provided the dendrites are exposed to similar synaptic inputs.

- Corollary to Rule 2. Axonal pathways form similar synaptic patterns onto all the dendrites of a single neuron, provided the dendrites occur within the target region of the axonal pathway.

- Rule 3. Neuronal types receive characteristic patterns of synaptic connections; the actual numbers, proportions, and spatial distribution of the synapses formed by each neuronal type occur within a range of values.

- Corollary to Rule 3. Different extrinsic and intrinsic synaptic pathways form specific proportions of their synapses with different postsynaptic elements (spines vs. dendritic shafts, one cell type vs. another).

- Rule 4. The receptive field properties of every cortical neuron are shaped by the spatial and temporal integration of inputs from a variety of excitatory and inhibitory sources. Inputs from a single source cannot be the sole determinant of the receptive field properties of cortical neurons.

- Rule 5. Only a fraction of the synaptic inputs to a cortical neuron are activated at one time. Therefore, the receptive field properties of cortical neurons are transitory and are determined by the cortical circuitry active at a given time.

- Rule 6. Excitatory and inhibitory synaptic interactions between cortical neurons preferentially link neurons situated in close proximity to one another, and these interactions typically link neurons having similar receptive field properties. Synaptic interactions between closely spaced neurons, having similar receptive field properties, provide a basis for the similarity of receptive field properties of neurons within a functional column.

Finally, it is important to note that the principal inputs received by any cortical column come from other cortical areas. It has been estimated that only 1 in 100 or even 1 in 1000 fibers in the white matter are involved in subcortical projections (thalamus and basal ganglia) [12]-[13]. The remaining white matter fibers are involved in intra- and inter-hemispheric connections from one

part of the cortex to another. It is thought that all cortical inter-columnar connections are reciprocal, i.e. that a cortical area receiving input from another cortical area also signals back to that area. The substantial majority of these cortico-cortical connections target pyramidal cells. In contrast, thalamic afferents target inhibitory interneurons as well as pyramidal neurons (see figures 2 and 3). Although the thalamus projects to all layers of the cortex, its most dense projections are to layers IV and VI, where they form about 5% to 10% of the synapses in those layers [13]. In addition, more than 20 other subcortical structures project to the neocortex. At present we have no simple schematic of these pathways, although the monoaminergic innervation of the cortex (metabotropic synapses using dopamine, norepinephrine or serotonin as the neurotransmitter) has perhaps been the most studied. The monoaminergic connections are modulatory rather than "data pathway" signals. One of their roles – and perhaps their primary role – is to modulate the level of excitability of cortical neurons, typically over a relatively large area involving a multiplicity of functional columns.

IV. Cortical Neurons

Although the classification of cortical neurons into four basic signaling types might seem to imply a certain simplicity in cortical signal processing, this is misleading. There is a surprising diversity of different morphological classes of cortical neurons, and each of these classes contains a multiplicity of subclasses. Different groups of authors do not even seem to agree on a common naming system for describing these different classes. Nonpyramidal neurons have been extensively surveyed by Fairén et al. in a comprehensive comparative anatomical review [14]. Toledo-Rodriguez et al. have presented a less comprehensive review of cortical neurons [11], which we summarize in table I.

Table I hints at the underlying diversity of cell types in the neocortex. Even so, it does not convey the full story. For example, within the general class of regular spiking (RS) responses, there are still more subtle differences. Most RS pyramidal (PC) and spiny stellate cells (SSC) show weak accommodation (that is, in sustained firing patterns the firing rate gradually decreases slightly), but some subpopulations in layers IV-VI show strong accommodation (that is, in sustained firing patterns the firing rate rapidly and significantly decreases). [11] documents a number of subclasses of signaling characteristics for the inhibitory neurons as well.

Different cortical neurons can co-localize neuropeptide neuromodulators as well. For example, a PC neuron of the RS class in table I can co-localize somatostatin (SOM) with its glutamate neurotransmitter, or it can co-localize cholecystokinine (CCK) but not both simultaneously, and it might not co-localize either one. This points to the possibility of different behaviors by neurons of

Table I: Brief Summary of Cortical Neuron Classes

Cell Type	Signaling Class	Primary Neurotransmitter	Co-localized Neuropeptide	Location of Cell Body	Dendritic Location	Principal Axonal Targets
PC	RS	glutamate	SOM, CCK	layers II-VI	all layers	WM, dendrites.
PC	IB	glutamate		V	all layers	WM, dendrites.
SSC	RS	glutamate		IV	IV	dendrites in II-IV.
LBC	FS, RS	GABA	NPY, CCK	III, V		soma and proximal dendrites with sparse intra-laminar and intra-columnar projections and long inter-columnar projections.
SBC	FS, RS	GABA	VIP, CCK	III-V		local soma and proximal dendrites with dense intra-laminar and intra-columnar projections.
NBC	FS, CB, RS	GABA	NPY, SOM CCK	III, V		local soma and proximal dendrites with sparse to dense intra-laminar and intra-columnar projections.
BTC	FS, CB, RS	GABA	SOM, CCK, VIP			intra-columnar over all layers
BPC	FS, IS, CB, RS	GABA	VIP	II-IV	all layers	dendritic shafts over all layers but few and very restricted target cells.
e-BPC	?	glutamate?	?	II-IV	?	dendrites.
DBC	FS, CB	GABA	VIP	II/III	?	dendrites over all layers in a column.
e-DBC	?	glutamate?	?	II-V	?	dendrites.
NGC	FS	GABA		I, III/IV	local layer	dendritic shafts in the same layer, column.
MC	FS, CB, IS	GABA	NPY, SOM CCK NPY+SOM	VI	VI+?	dendrites with intra-laminar and intra-columnar projections and inter-columnar projections.
CRC	?	GABA		I	I	local dendrites.
ChC	FS, CB	GABA		III, V	III, V/VI	local axons in same layer and column.

PC=pyramidal cell; SSC=spiny stellate cell; LBC=large basket cell; SBC=small basket cell; NBC=nest basket cell; BTC=bitufted cell; BPC=bipolar cell; e-BPC=excitatory bipolar cell (putative); DBC=double bouquet cell; e-DBC=excitatory bitufted cell (putative); NGC=neurogliaform cell; MC=Martinotti cell; CRC=Cajal-Retzius cell; ChC=chandelier cell; RS=regular spiking; FS=fast spiking; CB=continuous bursting; IS=irregular spiking; GABA=gamma aminobutyric acid; NPY=neuropeptide Y; VIP=vasoactive intestinal peptide; SOM=somatostatin; CCK=cholecystokinine; WM=white matter.

even the same general morphological class.

The presence of neuropeptides in the synaptic terminals of cortical neurons greatly complicates the picture insofar as signaling action by individual neurons is concerned. The onset of metabotropic second-messenger reactions due to the binding of a neuropeptide to a receptor in the postsynaptic cell is slow to begin, but the modulatory effects are generally very long lasting.

This has significance for understanding binding codes in the cerebral cortex. The situation is further complicated by the fact that neuropeptides have not received anything approaching the theoretical or the experimental treatment that has been applied to the various ion channels and their signal modulation effects (e.g. various Na^+, K^+ or Ca^{2+} ion channels that give different neurons their different basic signaling properties).

The effect of somatostatin (SOM) on the postsynaptic cell is generally inhibitory. SOM hyperpolarizes the postsynaptic cell by opening K^+ channels, thus depressing the ability of the postsynaptic neuron to respond to action potential (AP) signals [15, pp. 214-217]. It is thought that the half-life of SOM is on the order of less than 3 minutes. CCK acts on the postsynaptic cell via the phosphoinositol second messenger system (PhS) [15, pp. 393-400], [16], stimulating the production of diacylglycerol and raising intracellular levels of Ca^{2+}. The metabotropic reactions of the PhS are widely varied, and it is not known in detail what the precise effect of CCK on cortical neurons is. However, a common effect of the PhS on postsynaptic cells tends to be excitatory (e.g. phosphorylation of AMPA receptors, which increases their sensitivity). The vasoactive intestinal polypeptide (VIP) acts through the cAMP second messenger system [16], [17] and is known to have both excitatory and inhibitory effects [15, pp. 400-402]. The effects of neuropeptide Y (NPY) in the cerebral cortex are not well documented, but provisionally appear to be inhibitory. NPY receptors in the central nervous system belong to the superfamily of G protein binding receptors that interact with the G_i protein, which reduces levels of cAMP [15, pp. 419-421]. Reduction of cAMP is usually linked to inhibitory effects on postsynaptic response.

In summary, there is simply too little presently known about the effects of these different neuropeptide modulators in the cerebral cortex. It seems to be a reasonable guess that synaptic release of the neuropeptides is likely to be less probable than release of the small molecule neuro-transmitters with which they are co-localized, thus implying that neuropeptide release would be stimulated by sustained AP bombardment but not occasional AP events. However, this is mere speculation at this time. SOM and NPY are probably inhibitory. The effects of CCK and VIP are probably mildly excitatory [13]. But we simply do not have sufficient experimental data to predict exactly what the roles of the neuropeptides are in the cerebral cortex. What we can say with some degree of confidence is: Whatever these effects may be, they are slow to onset and relatively long-lasting compared to normal synaptic transmission of signals.

Whatever may be the effect of neuromodulation in cortical neurons, their normal synaptic signaling properties are much better understood. Wilson [4] has provided computationally efficient models for cortical neuron firing for the four major classes of cortical neurons. Figure 4 illustrates the behavior of the RS-class response, a category that includes pyramidal neurons and

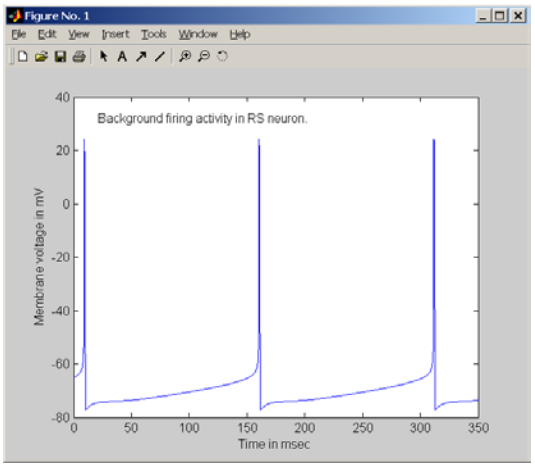

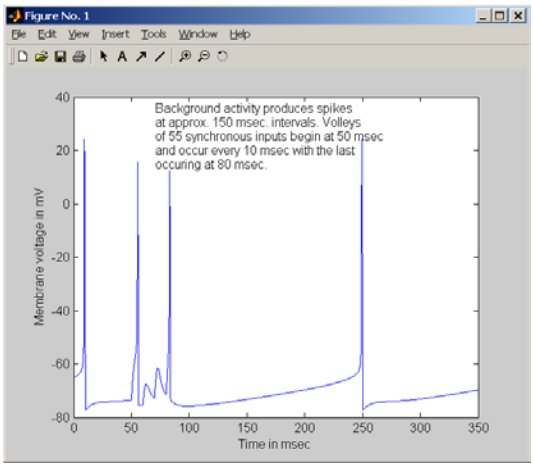

A B

Figure 4: Background and stimulated firing activity for an RS-type neuron. A. Background excitation set to produce AP responses at approximately 150 msec intervals (6 pulses per second background firing of the neuron). Note the pronounced after-hyperpolarization (AHP) following each AP. This is the mechanism for firing rate accommodation in the RS-type neuron. B. Response of the same neuron to synchronous volleys of 55 synaptic inputs each, spaced at 10 msec. intervals, beginning at 50 msec. with the last volley occurring at 80 msec. Note that the AHP prevented firing in response to the volleys at 60 and 70 msec.

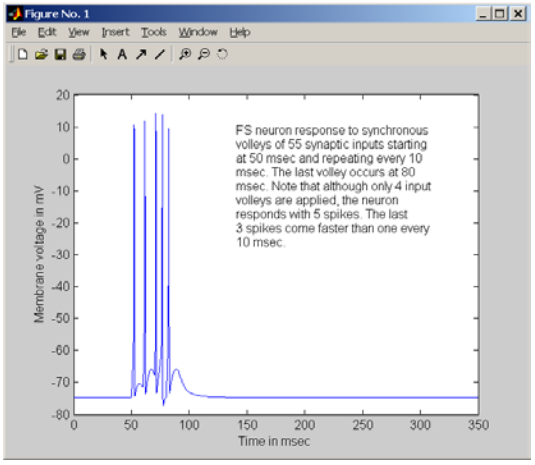

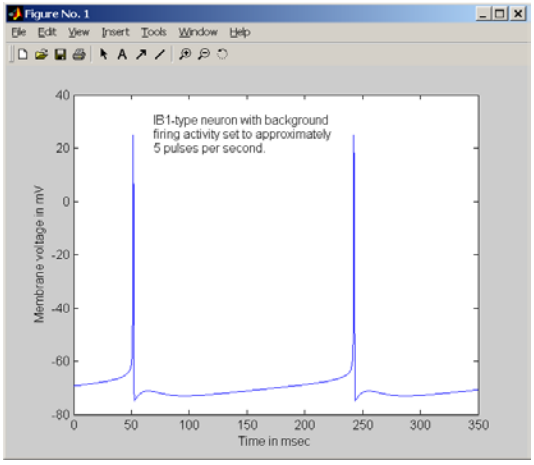

Figure 5: Response of the FS-type neuron to 4 synchronous volleys of 55 APs beginning at 50 msec. and occurring every 10 msec. The last of the volleys occurs at 80 msec. Note that although there are only 4 incoming volleys, the neuron has 5 AP spikes in response. The final 3 are at a rate faster than once every 10 msec.

Figure 6: IB subtype 1 neuron with background firing rate set to approximately 5 pulses per sec.

spiny stellate cells. It has been estimated [18] that under typical quiescent conditions pyramidal cells exhibit normal background firing in response to unsynchronized input activity at a rate of about 5 pulses per second. This is illustrated in figure 4A, where a background firing parameter has been set in the Wilson RS model in order to produce the background firing activity level. The

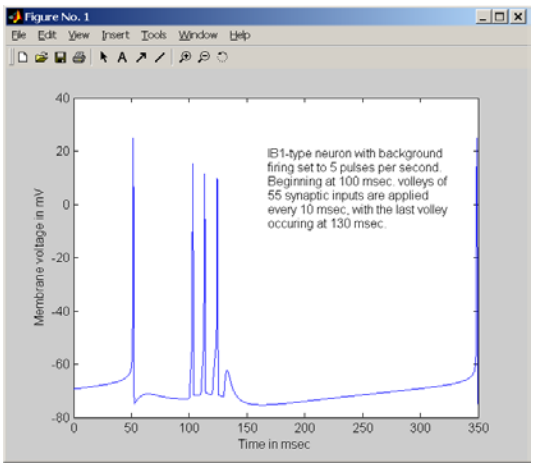

Figure 7: IB subtype-1 neuron response to four synchronous volleys of 55 synaptic inputs. The first volley occurs at 100 msec. and come every 10 msec. The last volley occurs at 130 msec. Note that although 4 volleys are received, the neuron responds only to the first 3.

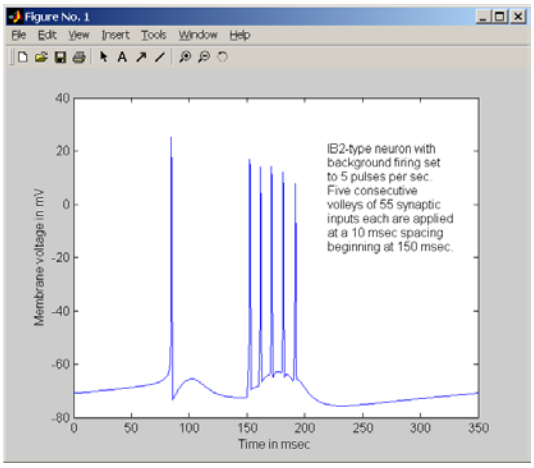

Figure 8: IB subtype-2 neuron response to five synchronous volleys of 55 synaptic inputs with the first volley coming at 150 msec. Background firing rate was set to 5 pulses per second. Note that the neuron responds to all 5 of the five volleys. It was observed that at slightly higher levels of background excitation the neuron responds with two background pulses rather than with one.

B figure illustrates the RS response to a volley of 4 consecutive synchronous inputs, spaced 10 msec. apart, equivalent to 55 simultaneous synaptic inputs each. Note that the neuron fails to respond to the second and third volleys. This is due to the pronounced after-hyperpolarization (AHP) mechanism present in RS-type neurons. The AHP mechanism is what causes their firing rate accommodation behavior, and which limits the maximum firing rate of RS-type neurons.

Most inhibitory neurons, on the other hand, belong to the FS-type category. These neurons are easily stimulated, do not accommodate their firing responses, and produce high-rate output pulses in response to stimulation. In figure 5 we illustrate the FS-type response to the same volleys as applied to the RS neuron in figure 4. Background firing activity for the FS neuron was assumed to be zero. This is because of two factors. First, there are far fewer inhibitory neurons in a functional column (approximately 15% of the population), and these synapse mostly to local pyramidal cells. Therefore we expect less background activity being received by these neurons. Second, FS neurons have a more "hair trigger" response and, consequently, do not appear to be statistically capable of the same low background firing rates as observed for PC neurons. Note in figure 5 that although the FS neuron received only 4 input volleys, it responded with *5* action potentials. The final 3 APs were emitted at a rate faster than the 10 msec input volley rate.

Figure 6 illustrates background firing activity for Wilson's IB-subclass 1 neuron. Intrinsic bursting neurons are not spontaneous bursters, and the activity in figure 6 is due to random (non-

synchronous) input signals. These have been adjusted to produce 5 pulses per second background firing. Figure 7 illustrates the response of this neuron to 4 synchronous input volleys (the same as used for the previous figures) beginning at 100 msec. Note that the neuron does not respond to the final input volley. This is due to the voltage-gated channel mechanisms responsible for bursting behavior in this neuron. There is a limited firing time for IB-class neurons, and figure 6 illustrates this. Wilson also models a second subclass of IB neuron, and this is illustrated in figure 7. This neuron had its background firing level adjusted to 5 pulses per second. It received a tetanus of five consecutive synchronous volleys (same parameters as in the other cases) spaced at 10 msec intervals and beginning at 150 msec. Note that this neuron responded to all 5 volleys. Note also the distinct difference in the neuron's repolarization dynamics as compared to IB subclass 1.

The clear lesson from this is that the physiological firing characteristics of the neurons in a functional column determines the manner in which this column can act as a synchronized assembly of cells. (In the next section we will briefly review the experimental evidence behind the hypothesis that functional columns act as synchronized oscillators in the neocortex, and that the synchronization of their firing patterns constitutes a possible binding code for object representation in the cortex. The section after that reviews some of the theoretical structures, the so-called population code models, that have been proposed as models of cortical synchronization). The firing patterns of such assemblies will clearly depend on the firing rates possible for neocortical neurons and upon the intensity of input activity needed to achieve them.

As an illustration of this point, figure 9 depicts two different firing responses of an RS-type neuron receiving volley inputs of different strengths at an interval of 20 msec. between volleys.

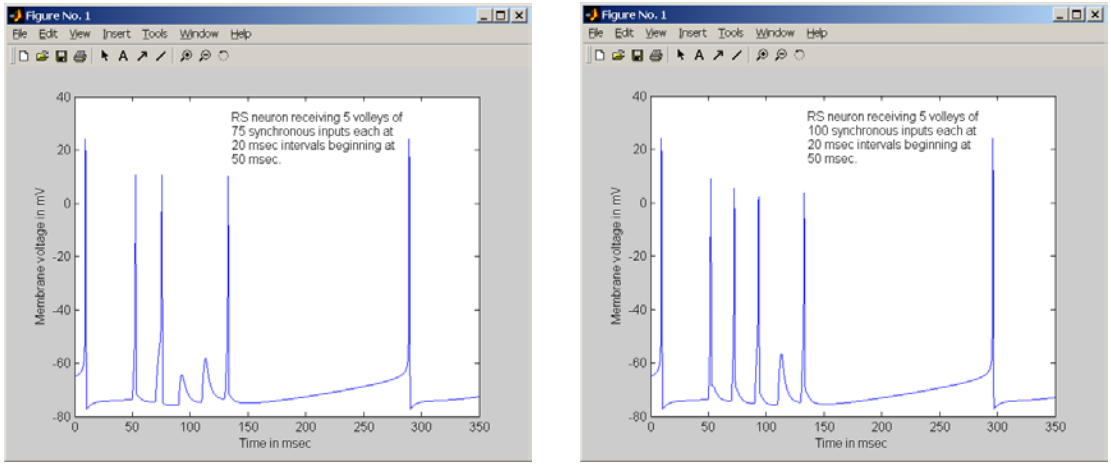

A B

Figure 9: Response of an RS neuron to different strength volleys at 20 msec. spacing between volleys. A. Response to volleys of 75 synchronous synaptic inputs. B. Response to volleys of 100 synchronous synaptic inputs.

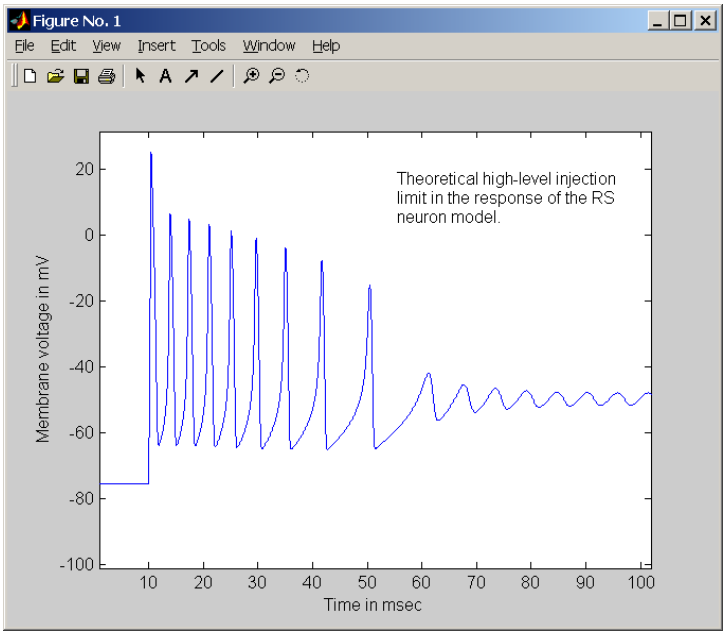

Figure 10. Theoretical high-level current injection limit in the response of the RS neuron model. A constant current of 2.5 nA is injected at 10 msec. The response is initially an accommodating high-frequency burst of action potentials. This response gives way to a depolarized membrane potential of approximately –50 mV after 40 msec of firing. No additional action potentials are generated thereafter. The initial interval between the first and second APs is approximately 4 msec., and this interval increases continuously until the burst dies out.

With 75 synchronized synaptic inputs (figure 9A), the neuron can respond fully to the first two volleys, but then its accommodation dynamics suppresses response to the next two. The neuron is able to respond to the fifth volley. With 100 synchronized synaptic inputs (figure 9B) the neuron responds to the first three volleys, suppresses the fourth, and responds to the fifth. Volley suppression for volleys received at less than 20 msec. intervals is even greater (see figure 4B). Computer simulations indicate that the RS neuron can achieve a steady firing rate on the order of 80 Hz (12.5 msec intervals), but it cannot sustain this rate unless the later volleys come in with a higher number of synchronized synaptic inputs than we have shown here. Note too that these results have not accounted for inhibitory action by the column's GABA-ergic neurons. The RS neuron can achieve very short bursts at higher firing rates than this, but it cannot maintain this higher rate for more than a few tens of milliseconds. Figure 10 illustrates the behavior of the RS neuron in the limit of high levels of constant current injection. Although initially the neuron responds with very high frequency spiking (approximately 4 msec between the first and second APs), this initial rate cannot be maintained, and after 40 msec of firing activity the spiking response ceases altogether. (Note that the mathematical model of the RS-type neuron does not address the issue of whether such a high level of current injection would kill the cell).

Based upon experimental estimates of neuron density in the cerebral cortex [19] and the estimated sizes of functional columns, a single functional column is likely to contain tens of thousands of neurons. Therefore a population-code modeling approach is probably a practical necessity in cortical modeling. However, confidence in a population model cannot be argued merely on the grounds that its underlying dynamical equations are simplified versions of 'neuron-like' responses (e.g. a Morris-Lecar-like model [20] or a 'thalamic-neuron-like' model [21]). This is especially the case when, as has often been the practice, the population model takes a 'one-size-fits-all' approach to the 'neurons' used in its population element model. There is no a priori reason to suppose that the emergent behavior of a large assembly of neurons is a direct mirror of an individual neuron's dynamics.

V. Synchronized Oscillation and Wave Activity in the Neocortex

In 1981 Christoph von der Malsburg proposed the idea, regarded as radical and speculative at the time, that object representation in the neocortex was constituted by a temporal code of correlated and synchronized firing activities involving multiple and reconfigurable assemblies of cells [22]. Von der Malsburg's hypothesis was slow to catch on and is still somewhat controversial today. It did not begin to attract widespread serious attention until the late 1980s and early 1990s when experimental evidence pointing to the existence of synchronized oscillations in the neocortex began to emerge from various laboratories [23]-[27]. Also during this time other challenges were being mounted in opposition to the conventional thinking about cortical organization of the time. On the basis of studies of patients who had suffered bilateral damage to the rostral integrative cortices, anterior temporal lobe damage, anterior frontal lobe damage, and damage to single-modality sensory association cortices, neurologist A.R. Damasio proposed that binding of entities and events in the brain depended on time-locked multi-regional *retro*activation of neural groups by means of small assemblies of neurons he called "convergence zones" (CZs) [28]-[29]. In Damasio's model, signal propagation is both caudo-rostral from sensory cortices toward the frontal lobes *and* vice versa. Pathways converge, level by level, at convergence zone networks, which feed back directly to their immediately upstream sources and feed forward to immediately downstream CZ targets. Projections from the hippocampal system and other non-cortical circuits in the basal forebrain, brain stem and neurotransmitter nuclei facilitate multiregional time locking. Damasio's model, illustrated in figure 11, stood in sharp contradiction to the earlier (and still adhered to by many) model of caudal-to-rostral information flow within the brain, in which the successive integration of information increases in complexity and detail as one progresses from the rear (caudal) areas of the brain toward the frontal (rostral) areas.

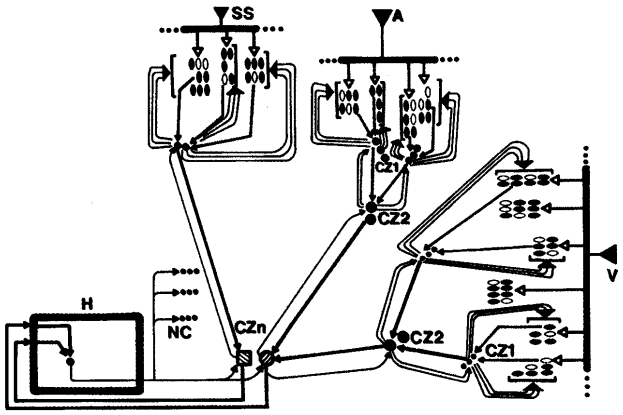

Figure 11: Damasio's model of neural organization. In his hypothesis, signals from upstream neural assemblies converge on small assemblies of neurons dubbed convergence zones (CZs). A CZ provides feedback signals directly to those upstream assemblies that directly converge upon it. This rostral-to-caudal feedback is also presumed to be capable of re-stimulating these regions even in the absence of direct sensory stimulus (thereby providing a neural substrate for the capacity of 'imagination'). CZs also project signals downstream to 'higher level' CZs, which in turn project retroactive feedback to them. There is further and more non-specific involvement by non-cortical regions of the brain (e.g. the brain stem) and subcortical regions, particularly the hippocampal system. Convergence zones are presumed to produce spatio-temporal binding codes that produce time-locked synchronous activity in various 'feature-fragment-representing' regions of the early sensory cortices. Objects are supposed to be represented by this synchronized signaling activity. V=visual cortex; A=auditory cortex; SS=somatosensory cortex; NC=non-cortical nuclei; H=hippocampal system.

Early models proposed for temporal coding employed a very simple picture of synchronized pulse trains. Theoretical arguments for this model were advanced by Abeles in the form of "synfire networks" based upon known physiological properties of neuron excitability and statistical models of network behaviors [18]. Many of these models more or less implicitly assumed that synchronization was driven in the caudal-to-rostral direction with little explicit role given to feedback signals returning upstream to the early sensory cortices. Due to technological limitations at the time, the synchronization model had to be inferred from single-unit recordings, and the activity of neural populations had to be inferred from this data. Most of the early thinking directed at the synchronization model largely conformed to the traditional neuroscience view that information processing in the brain takes place hierarchically in the caudo-rostral direction. Although it was known that neural feedback connections are common in the neocortex, it was nonetheless supposed that by and large object and event representation was by means of a "synfire-like" and primarily feedforward organization. Naturally, this new hypothesis did not immediately gain the assent of the neuroscience community at large. The binding-by-synchronization hypothesis has been experimentally tested through psychophysical and spike-recording experiments. Results from these studies lead some researchers to challenge the hypothesis [30]-[33]. However, these findings were not conclusive and explanations have been

put forth in answer to the criticisms that have been raised [34]-[37].

Strangely enough, Damasio's hypothesis has received very little follow up work by experimentalists. Although it has long been accepted that any two areas of the cerebral cortex that signal to each other do so reciprocally, and despite the experimental evidence presented below, there has been no concentrated effort to confirm or refute Damasio's convergence zone hypothesis. What relatively little experimental work has been carried out has been mainly of a psychological nature and has focused primarily on one piece of Damasio's proposal, namely those convergence zones that he dubbed "somatic markers" [38]-[39]. Not surprisingly, most of the work supporting the model has been carried out by Damasio and his associates, e.g. [40]-[41]. Some lukewarm support has also been reported independently by Lösel and Schmucker [42]. Some indirect possible support for the PET scan studies of Damasio and his coworkers has also been seen by Burgess et al. [43], although their paper makes no remarks linking their data on the ventromedial prefrontal cortex (Brodmann's area 11) with [41].

Experimental evidence for the existence of oscillator-driven traveling wave phenomena in the neocortex has found firmer empirical footing [23]-[24], [26], [44]-[48]. Of course, the existence of neural oscillators, such as the central pattern generator, has long been recognized. Much of the work in this area has been carried out in connection with invertebrates or with subcortical regions of the vertebrate brain. The confirmation of oscillator mechanisms in the neocortex, and the accompanying evidence for traveling waves of activity over large regions of the neocortex, is of much more recent vintage. In a tradition developed from EEG methods, oscillation phenomena is typically divided into four frequency bands: 1) the low frequency band (0-3.5 Hz); 2) the alpha band (7-14 Hz); 3) the beta band (14-28 Hz); and 4) the gamma band (28-80 Hz).

Figure 12 illustrates the traveling wave phenomenon in the gamma band in monkey visual cortex [45]. This data was recorded from a linear array of microelectrodes spaced at a pitch of 0.5

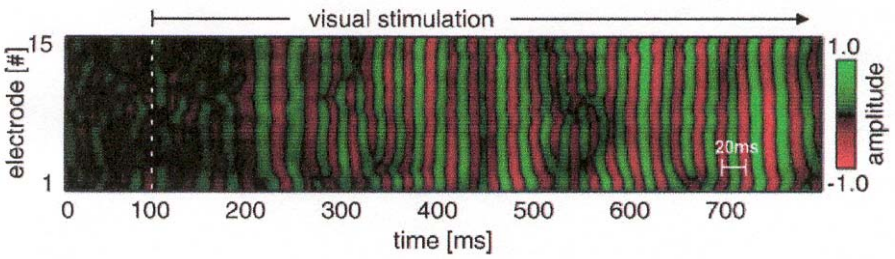

Figure 12: 15-channel recording of gamma-band signals in striate cortex of an awake monkey. Data was recorded from a linear array of microelectrodes spaced with a 0.5 mm pitch. Visual stimulus was applied beginning at 100 msec. The illustration is taken from [45]. Gabriel and Eckhorn interpret the results as indicative of a broad wavefront, interpreted to be a traveling wave, arriving nearly simultaneously at the fifteen different microelectrode positions.

mm. The data was bandpass filtered in the 30-70 Hz (gamma band) frequency range. Gabriel and Eckhorn interpreted this result as indicative of a traveling wave with a broad wavefront arriving simultaneously (or nearly simultaneously) at each location. The details of this particular measurement method reported in [45] are somewhat imprecise. For example, it is not explained why the result is regarded as a traveling wave rather than as indicative of a standing wave. The general mathematical form of a one-dimensional traveling wave traveling in the +*x* direction is

$$y_r(x,t) = u(x - vt)$$

where *u* is some function and *v* is the wave velocity. The general form of a wave traveling in the opposite direction is

$$y_l(x,t) = u(x + vt).$$

The simplest example of a traveling wave is that of a traveling sinusoid

$$y_r(x,t) = \sin(kx - \omega t)$$
$$y_l(x,t) = \sin(kx + \omega t)$$

for waves traveling to the right or left, respectively. Here *x* is position, *t* is time, *k* is spatial frequency ($2\pi/\lambda$, λ = wavelength), and ω is the temporal frequency in radians/sec. The temporal and spatial frequencies are related to each other as $\omega\lambda = 2\pi v$. If figure 12 is representative of a wavefront, this is equivalent to saying that the *x* position is the same for all the electrodes. In this case, the result is not distinguishable in time from a standing wave

$$y_s(x,t) = y_r + y_l = 2\sin(kx)\cos(\omega t)$$

since the *x* variable would be constant. In order to unambiguously distinguish a traveling wave from a standing wave, a two-dimensional grid of microelectrodes would be required.

Due to technology challenges in making measurements of cortical activity, it is often a matter of interpretation whether the data is indicative of a traveling wave or a standing wave phenomenon. Indeed, many descriptions are reported qualitatively rather than quantitatively. Because quantitative measurements of wave characteristics in neural systems are rather heavily laden with mathematical signal processing necessary to extract the pertinent quantitative data, how the wave is interpreted, i.e. as a traveling vs. a standing wave, is crucial. This is because the mathematical signal processing to be employed and the interpretation of the results depends on whether one assumes a $y(x, t)$ of the form given above or of the form $u(x\text{-}vt)+u(x+vt)$. For instance, in [45] it is assumed that $y(x, t) = u(x\text{-}vt)$, and this assumption sets up the mathematics of the data extraction in that paper.

Neuroscientists involved in this area of research typically are willing to accept the traveling wave interpretation of the data in figure 12, but [45] does provide a noteworthy example of an

instance where the reader cannot be altogether sure that the traveling wave interpretation is not an instance of the experimenter seeing what he expects to see. It is known that traveling waves, or, more accurately, traveling wave *packets*, do appear in some central systems. One example is a slow traveling wave observed in the procerebral lobe of *limax*, a structure responsible for olfactory processing in this slug [49]. However, this does not mean that all wave-like phenomena, such as figure 12, are necessarily traveling-wave phenomena, especially when one considers the existence of retroactive (that is, reciprocal) coupling from 'downstream' regions back to 'upstream' regions. Nonetheless, it has been established that the wave phenomena is a fact descriptive of cortical behavior [50]-[55].

Waves in biological systems, unlike the more familiar waves of mechanical or electromagnetic systems, propagate in a thoroughly inhomogeneous medium, namely neurons (and glial cells[1]). Among other things, this means that wave velocity is not necessarily a constant within this medium. Thus, the 'wave mechanics' of neural systems is considerably more complicated than that of the more familiar mechanical or electromagnetic systems. In the next section we will take a look at some of the approaches being tried in the attempt to understand these nonlinear wave mechanics.

The waves with which we are here concerned are 'activity waves,' i.e. spatially and temporally distributed firing activities of neural assemblies. Now, a wave can be regarded as a large-scale cooperative phenomenon. It is no longer a question of whether or not wave behavior is characteristic of neural systems. The question is whether or not synchronized or coherent waves of neuronal activity constitute a form of information representation, i.e. a neural code. This is the famous **binding code hypothesis** and it is at the forefront of present day research. Therefore we are bound to ask, "What properties of activity wave phenomena are to be examined as possible forms of information representation in large-scale neural systems?"

V.A: Mathematical definitions of wave properties.

There are two such properties that presently command the attention of researchers. These are called **synchrony** and **phase continuity**. Both require us to understand the concept of "phase" in wave phenomena. As used in signal processing theory, phase[2] refers to the relative alignment of two periodic signals. In the simplest case these two signals have the same fundamental frequency

[1] Glial cells do not, of course, produce action potentials. However, it has been established in recent years that networks of glial cells do propagate calcium throughout broad regions of the cortex and do so in waves (so-called 'calcium waves'). This particular wave phenomenon will not concern us further in this paper.
[2] The term "phase" has various meanings in different fields of science. For example, in the study of matter or in thermodynamics the term is used in such contexts as "solid, liquid, and gas." In signal processing theory the definition of "phase" is at root purely mathematical.

(the reciprocal of the period of the signal). One period of the signal is said to correspond to an angle of 2π radians. Thus, for a period of T seconds and a frequency of ω radians per second, we have $\omega T = 2\pi$. At every time t a periodic signal is said to have an angle $\theta = 2\pi t/T$. The relative phase of two signals, y_1 and y_2 is the angle $\phi = \theta_1 - \theta_2$.

As a simple example, let us take two signals of the form $y_j(x_j, t) = \sin(kx_j - \omega t)$, $j = 1, 2$. The phase between these signals is easily found to be $\phi = k(x_1 - x_2) = \omega(x_1 - x_2)/v$ where the symbols are as defined earlier. The two signals are said to have **in-phase synchrony** if ϕ is an integer multiple of 2π, and are said to have **anti-phase synchrony** if ϕ is an odd integer multiple of π (that is, π, 3π, 5π, etc.). This definition is easily extended to two different spatial positions in a periodic non-sinusoidal traveling wave provided that the wave velocity is constant. It can also be modified to apply to two independent signals (that is, two signals not necessarily belonging to a wave) provided that there exists a period T that is the least common multiple of their two periods. If their fundamental frequencies are equal, the two signals are said to be **frequency locked**. Otherwise they are **harmonically locked**. The relative phase ϕ is defined in terms of what is known as the phase delay, T_D. Let $y_1(t)$ be the lower frequency signal. Some reference point $y_1(t_0)$ is chosen (usually a peak value, a zero crossing point, a half-amplitude point, or some other easily identifiable value of y_1). A corresponding reference point is chosen for y_2 such that this point first occurs at time $t_0 + T_D$, $T_D < T$, and repeats over every time interval T in $y_2(t)$. The relative phase of y_2 with respect to y_1 is then defined to be $\phi = 2\pi T_D/T$.

If two signals are frequency or harmonically locked and ϕ is a constant, the signals are said to be "phase locked." If ϕ is non-zero, the signal whose reference value occurs first is said to "lead" the other signal and, conversely, the other signal is said to "lag" the former. If two signals are not frequency or harmonically locked, no meaningful definition of relative phase ϕ is possible and the signals are said to be "incoherent" with respect to each other. If the two signals have the same fundamental frequency and are phase locked, they are said to be "phase locked 1:1"; if the second signal has a fundamental frequency twice that of the other and they are phase locked, they are said to be "phase locked 2:1"; if $mT_1 = nT_2 = T$ (with m and n integers) they are "phase locked n:m" etc.

Next let us consider two points, x_1 and x_2, for the simple standing wave described earlier. Any location for which kx is an integer multiple of π is called a **node** and y_s is equal to zero at that point at all times t. What is the relative phase between any two points that are not nodes? From inspection, we can see that at every non-nodal point x_j we will have $y_s(x_j, t)$ reaching either its peak value or its negative peak value, depending on the sign of $\sin(kx_j)$, at the same time t,

namely whenever t is an even integer multiple of the period $T = 2\pi/\omega$. Likewise, y_s will equal zero at *every* point x whenever ωt is an odd integer multiple of $\pi/2$ because $\cos(\omega t) = 0$ at these values. Therefore, any two points x_1 and x_2 will always have either in-phase synchrony or anti-phase synchrony in a standing wave, depending of whether the signs of $\sin(kx_1)$ and $\sin(kx_2)$ are equal or opposite, respectively. A standing wave is therefore said to be **globally synchronized** (where we understand that any two points can be relatively in-phase or anti-phase with respect to each other depending on the distance between them).

Next let us define the term phase continuity. We consider signals distributed over a spatial region of many points and assume that every signal in this region is frequency or harmonically locked with every other signal. Between any three linearly contiguous points in space we can define relative phases. Let ϕ_{12} be the relative phase between signals at x_1 and x_2 and let ϕ_{23} be the relative phase between x_2 and x_3. Let θ_j be the phase argument of the signal at x_j so that $\phi_{12} = \theta_1 - \theta_2$, etc. The rate of change in phase with respect to spatial position is then defined to be

$$\frac{\Delta\phi_{12}}{\Delta x} \equiv \frac{\theta_1 - \theta_2}{x_1 - x_2}$$

and similarly for all other pairs of contiguous points. In the limit where we take Δx to go to zero (the 'continuum limit'), this expression becomes a derivative with respect to x. When we generalize our situation to two spatial dimensions, it is known as a 'directional derivative' and in the direction for which $\Delta\phi / \Delta x$ takes on its largest magnitude, it is known as the **phase gradient**. Our distributed set of signals is said to have **phase continuity** if the phase gradient is constant. This means that in the gradient direction the rate of change, $\Delta\phi / \Delta x$, does not change value.

All these definitions arise from classical signal theory, and they all depend on the signals under consideration being periodic. This raises special problems and issues when this theory is to be applied to neural systems because in many cases the activity of any particular neuron is usually not periodic. Consider the case where a class IB-type 1 neuron fires as shown in figure 13. There are two important factors at work in this neuronal firing pattern. First, the neuron fires only over a short interval of time. If it does not repeat this firing pattern at regular intervals, its signal is not periodic. Even within the firing activity shown in the figure, the neuron is not in the most strict sense firing periodically because the intervals between its pulses are not constant. The **instantaneous firing rate** of the neuron, defined to be the reciprocal of the time between pulses, is not constant. Even though the last five pulses in the figure have settled into a more-or-less constant firing rate (short term periodicity), the mathematical definitions given above cannot be directly applied without modification to define a phase between this and another similar signal.

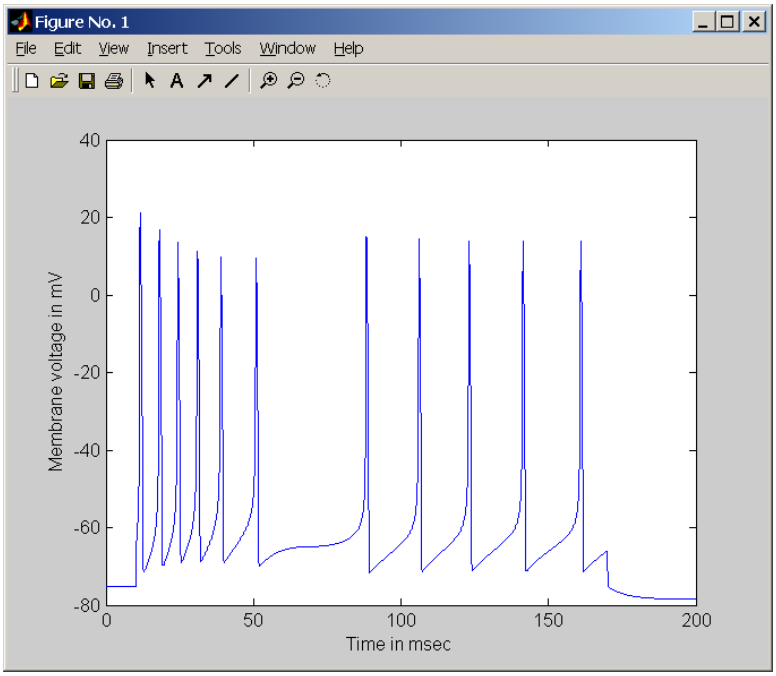

Figure 13: An IB neuron firing an aperiodic short burst of action potentials due to a dc current injection.

Consequently, it is often the case where either the classical definitions presented above must be modified or else the signals being compared must be somehow redefined so that the previous definitions can be applied. Unfortunately, there is no one universally-agreed-up definition for handling such cases and different researchers often do not clearly state which of the many possible 'operational' definitions of 'phase' they are using in their papers. Often these operational definitions must be made in the context of the measurement technique being used by the experimenter. These techniques can be broadly divided into time domain methods, frequency domain methods, and hybrid methods (involving both time and frequency). Because the root of the binding code hypothesis involves the notion of cooperative action among different assemblies of neurons in different locations in the neocortex, many researchers abandon the notion of phase altogether in favor of **correlation methods**, a more abstract notion of describing cooperative relationships (or the lack thereof) among different signals. We will next take a look at one very interesting recent example.

V.B. Eckhorn's envelope-to-amplitude method.

Experiments reveal that population activity in a local assembly of neurons is accompanied by changes in membrane potential across a broad spectrum of frequencies. Figure 14 illustrates measured high and low frequency variations in the membrane potential of a cell in the cat visual cortex [56]. In addition to the high frequency and spiking activity, we can note the low frequency

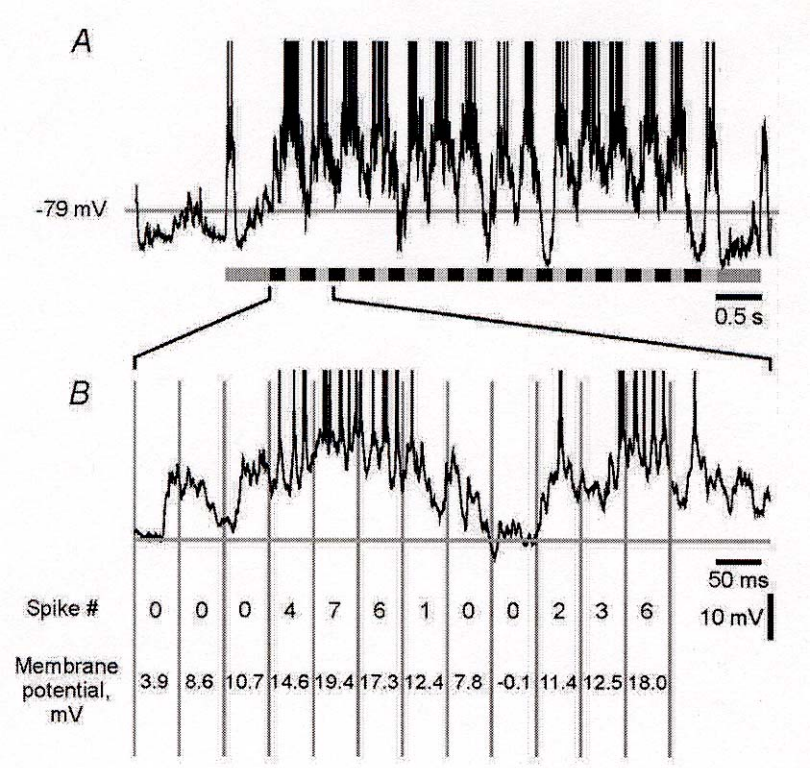

Figure 14: Experimentally recorded membrane potential of a neuron in the visual cortex of an anesthetized cat [56]. The data was recorded intracellularly using electrodes. The neuron type was not identified. The average resting potential, measured over 15 cells, was –67.3 ± 2.59 mV. For this cell the mean resting level was –79 mV. Mean resting potential is defined as the average membrane voltage averaged across all stimuli and all repetitions as well as over the 100 msec prior to stimulus presentation. A. Response of the cell to a moving grating presented monocularly to the dominant eye. B. Expanded scale from an epoch in A with measured deviation from mean resting potential and measured number of action potential spikes.

variations observed in the membrane potential brought about by stimulation of the cat's visual system. Volgushev et al. reported that both low frequency depolarization, as illustrated in the figure, and low frequency hyperpolarization could be produced by using different stimuli. They further reported that spike generation was more likely to occur when the cells exhibited high frequency oscillation in the gamma band than when such oscillations were not present. They also found that gamma band oscillations were stronger when the stimulus presented was one for which the cell appeared to be 'tuned' to respond to than they were for stimulus presentations that were 'non-optimum' for the particular cell. From their data analysis they concluded that the presence of gamma band oscillations in a cell corresponded to visual stimuli assumed to stimulate firing activity in the receptive field of the cell. It has elsewhere been reported that large (> 10 mV) low frequency fluctuations, lasting from 50 msec to more than 1 second, can be observed in cells in the cat visual cortex prior to and following stimulus onset [57]. The physiological cause of these bistable fluctuations was not ascertained in [57].

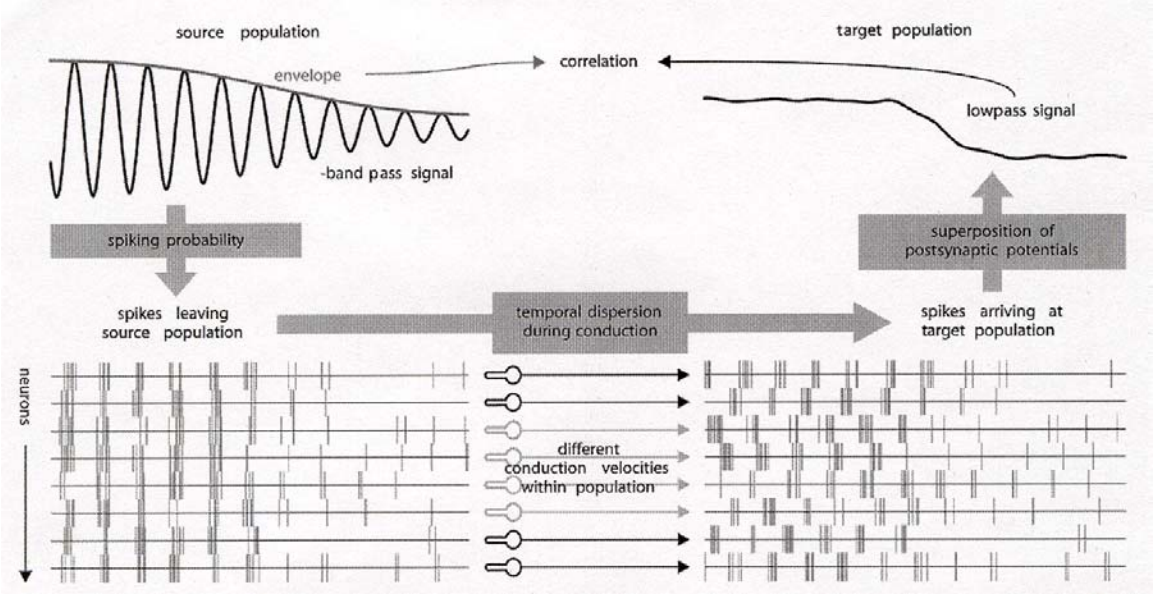

Figure 15: Gamma-envelope-to-low-frequency-correlation method proposed by Eckhorn et al. Spiking activity in a source population of neurons (lower left) gives rise to measurable gamma band oscillations picked up by EEG or subdural extracellular sensors (upper left). They propose that the amplitude of gamma band oscillations correlates to cell spiking probability while the phase of the oscillations (relative to a reference time and determined from measured phase delay) correlates to the average spike timing. During conduction of the action potentials to other regions of the cortex, variations in conduction velocity leads to dispersion of the arrival times of the spikes. This destroys correlation between gamma band signals at the source and gamma band oscillations at the destination (lower right). However, low frequency signals at the destination reflect average levels of cell firing and low frequency variations in regional membrane potential due to the received spike ensemble. They therefore propose that correlation measurements between low frequency signals at the destination and the envelope of the gamma band oscillations at the source is an indicator of region-to-region signaling in the cortex. The figure is taken from [58].

Based on these and other findings, Eckhorn et al. proposed a novel method for determining when different regions (different collections of functional columns in diverse places within the neocortex) are coupled. Their hypothesis is illustrated in figure 15 [58]. Their general argument goes as follows. Feature representation in an upstream source population of neurons is reflected in synchronized firing of action potential bursts in neurons within this assembly (figure 15, lower left). This synchronized firing activity can be detected extracellularly by EEG or intracranially by subdural electrode grids [48] and, in particular, is revealed as gamma band oscillations (figure 15, upper left). The amplitude of these gamma band oscillations is correlated to spiking probability within the source population, and the envelope of the gamma band oscillations changes as the average firing rate intensity varies within the source population.

Due to variations in conduction velocities along various pathways, these initially synchronized pulses become dispersed in time and arrive at a destination population more or less de-synchronized (figure 15, lower right). This dispersion destroys the phase coherence and gamma

envelope correlation between the source and destination populations [48]. However, the destination population still exhibits low frequency variations in the average membrane potential in the destination region (figure 15, upper right), and these low frequency variations can be correlated with the gamma band envelope at the source region. Consequently, they propose, gamma band envelope to low frequency signal correlation is an indicator of signal coupling between different regions of the neocortex [58]. The physical picture presented by this hypothesis is one that can be regarded as multi-path traveling wave propagation from the source population to the destination population. However, owing to the non-linear character of how arriving signals are recombined at the destination neurons, this multi-path traveling wave is not subject to the same type of wave-cancellation phenomenon seen in mechanical or electromagnetic multi-path signaling.

Bruns and Eckhorn have measured various types of correlations intracranially in human visual cortex using a subdural electrode grid [48]. The experimental subject was a female 18-year-old epilepsy patient undergoing pre-surgical evaluation and the experiment was conducted in the patient's hospital room with the patient awake and seated upright in bed. Figure 16 illustrates the locations of the electrodes in the grid, measured baseline time-frequency plots from two electrodes (B), and gamma-envelope correlations (C). We can note that the baseline cross correlations are quite low, although it is clear that there is more cross correlation within area A (see figure caption) than within area B or between the areas. We can effectively regard baseline area B as completely uncorrelated and likewise the inter-areal couplings are uncorrelated.

The measurements reported in [48] required quite sophisticated signal processing of the data, fully described in their paper. No assumption was made by this analysis as to the propagation modes for the signals, and in particular no wave-mechanical assumptions were employed. Bruns and Eckhorn measured several quantities, including statistical coherence, phase consistency (essentially a measure of synchrony), envelope-to-envelope correlation by frequency band (essentially the cross-correlation between envelopes in different locations in the same frequency band), and envelope-to-low-frequency correlation (the measure depicted in figure 15). Measurements were made for the alpha-, beta-, and gamma-frequency bands.

Bruns and Eckhorn found that coherence, phase consistency, and envelope-to-envelope correlations were maximal at zero time lag. (Zero time lag implicates temporal synchrony). Envelope-to-low-frequency-signal correlation (ELFS), on the other hand, was largely negligible at zero time lag and was maximum for area A to area B coupling at a time lag of 40 msec. ELFS correlation was the only measure that showed a correspondence to task- and event-related inter-areal activity.

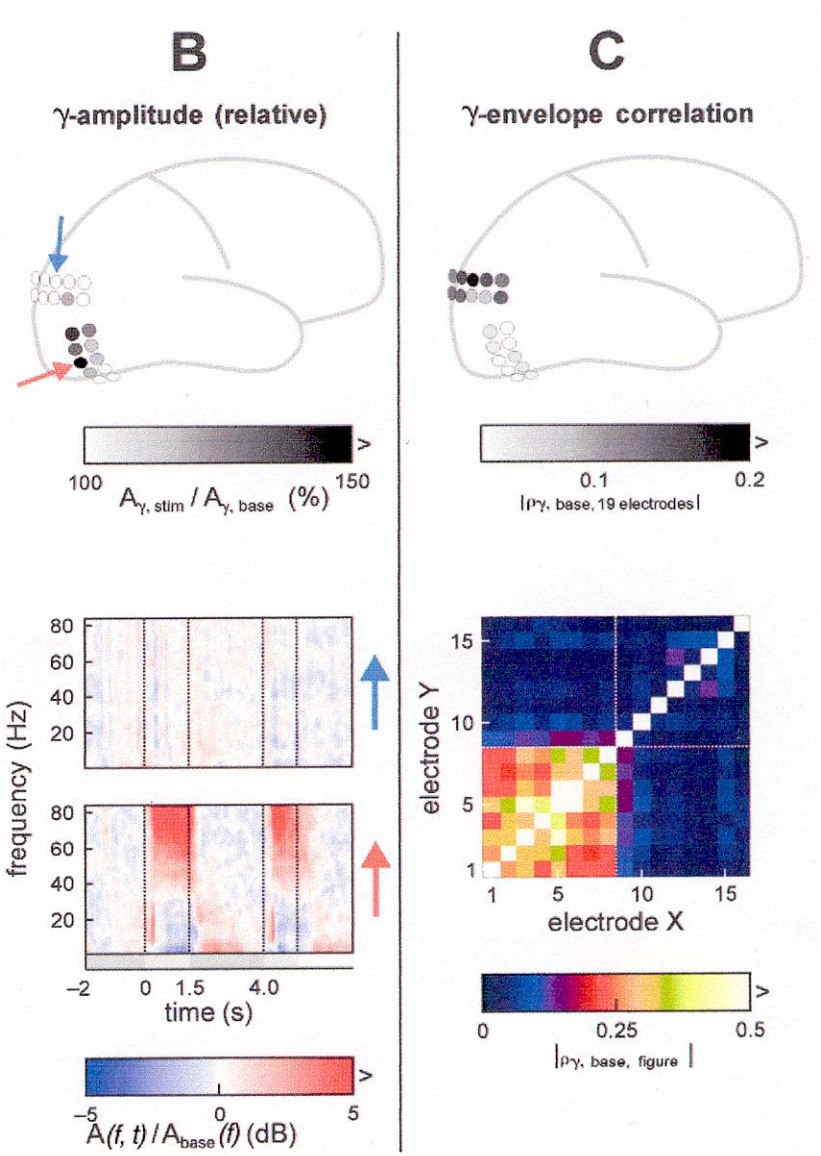

Figure 16: Electrode grid placement and baseline measurements of visual cortical activity [48]. Two visual cortical areas were examined (top of figure). Area 'A' is in the primary visual cortex, area 'B' was identified as the visual association cortex. Figure 16B shows relative spectral amplitudes and time-frequency plots for one grid in area A and another in area B. Figure 16C shows overall baseline correlation coefficients of gamma-band envelopes for the overall grid (top of figure) and cross-correlation coefficients between pairs of 16 different electrodes. Electrodes 1 – 8 are in area A; 9 – 16 are in area B. Dotted lines in the lower right figure mark the inter-areal border. The four quadrants represent inter-areal coupling from A to A (lower left), B to B (upper right), A to B (upper left), and B to A (lower right). Note that the cross correlation coefficients at baseline are generally quite low (except along the diagonal), but are higher within area A than within area B or for intra-areal couplings. The electrode numbering corresponds more or less with the order in which electrodes are encountered in moving from the most posterior/superior to the most anterior/inferior location. Electrodes had a contact diameter of 2.4 mm and were arranged in a rectangular grid with nearest-neighbor center-to-center spacing of 10 mm. The measurements therefore reflect a spatial summation over an area comprised of many functional columns.

The coupling patterns reported by Bruns and Eckhorn are shown in figure 17 for zero time lag for baseline activity. Bruns and Eckhorn reported that coherence, phase consistency and envelope

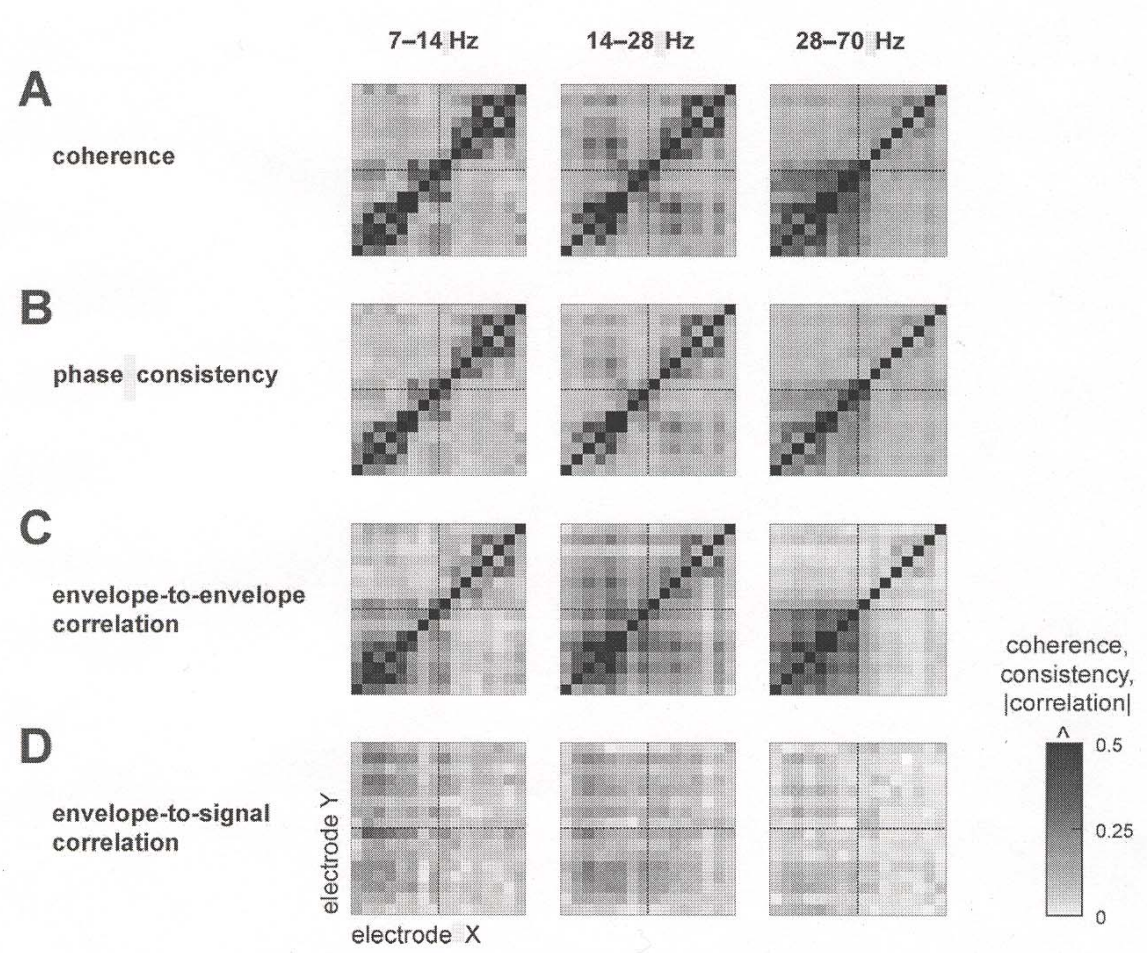

Figure 17: Various correlation measures among electrodes at zero time lag for different frequency bands. The figure is taken from [48]. The measurements were taken during baseline periods. Bruns and Eckhorn reported that measures A-C showed no prominent event- or task-related variations, while D (gamma band envelope to low frequency signal correlation, ELFS) did exhibit event- and task-related changes. Alpha band is 7-14 Hz. Beta band is 14-28 Hz. Gamma band is 28-70 Hz.

to envelope correlation did not show any prominent change in the results during event- or task-related activity. Maximum correlations for all three occurred at zero time lag, which is indicative of the degree of synchrony among signals at the various electrodes. Coherence and phase consistency averaged a cross-measure correlation of 0.98, indicating that these two measures are equivalent insofar as being indicators of synchrony or phase locking. Cross-measure correlation between coherence and envelope-to-envelope correlation was 0.88, and it was 0.83 between phase consistency and envelope-to-envelope correlation. None of these measures showed very high cross-measure correlation with envelope-to-low-frequency-signal (ELFS) correlation. Coupling patterns were most clearly structured with envelope-to-envelope correlation. They report that the only noteworthy event-related coupling changes were transient increases (about 500 msec in duration) within area B (see figure 16) in the alpha-band range after stimulus onsets,

and decreases within area A in the gamma-band range after stimulus changes (onsets and offsets). The measurements reported here are consistent with other findings that coupling within the gamma band of envelope-to-envelope correlation is restricted to a spatial range of only a few millimeters [47], [59]-[61]. Examination of the figure above appears to indicate that synchrony among nearby regions of the neocortex is exhibited principally in the alpha- and beta-bands, but not in the gamma-band outside of area A.

We now come to the main findings of [48]. Figure 18 shows the absolute value of ELFS correlation in the three frequency bands during experimental activities/stimulation. ELFS correlation was the only measure that exhibited prominent event- and task-related changes during the experiment. The maximum correlation occurred at a time lag of 40 msec. Looking at the second column in figure 18, inter-regional coupling between A and B was observed in the gamma- and beta-band frequencies. The coupling was highly asymmetric in the gamma band; there was significant A-to-B coupling between the envelope and the low frequency signal, but there was not a corresponding significant coupling from the envelope in the B region to the low frequency signal in the A region. Some B-envelope-to-A-signal coupling occurred in beta band.

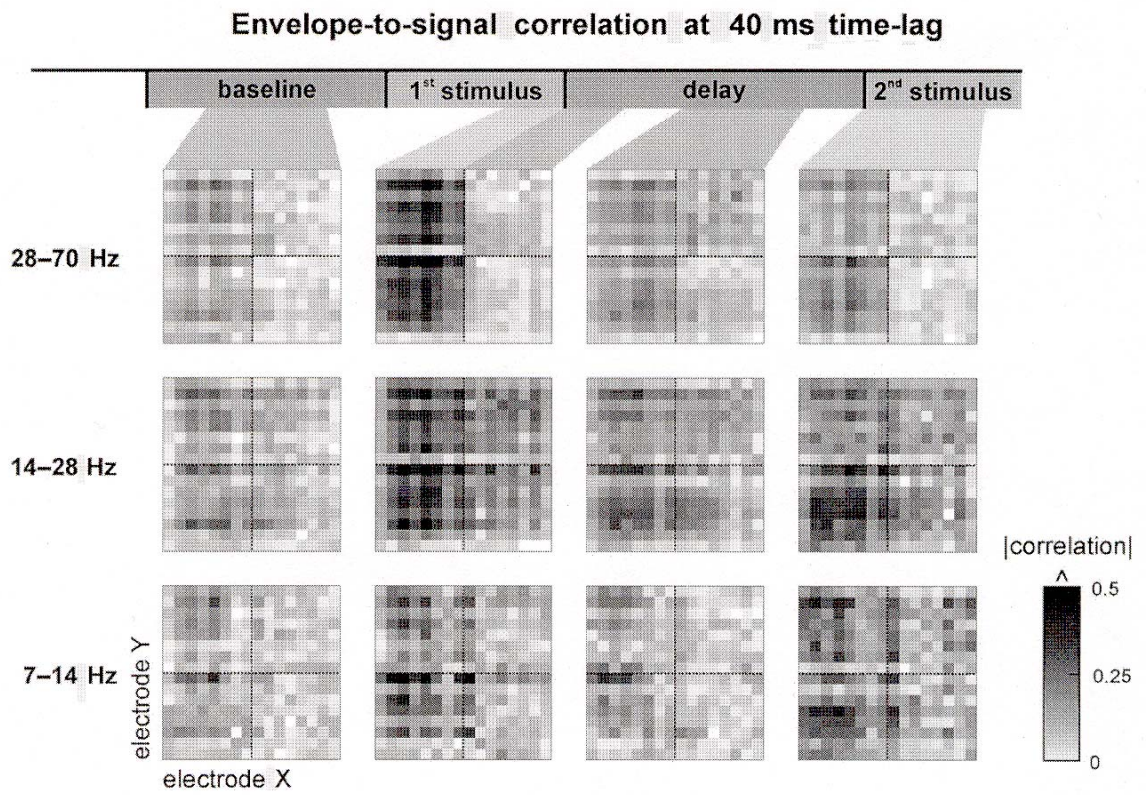

Figure 18: Absolute values of envelope-to-low-frequency-signal (ELFS) cross-correlations at 40 msec time lag during experimental activity. The figure is taken from [48]. Only the ELFS measurement showed significant event-and task-related variations.

The results shown in figure 18 are the principal evidence in support of Eckhorn's model of figure 15. Bruns and Eckhorn reported that the envelope always led the low-frequency signal, which seems to imply a causality relationship, i.e. that the low frequency signal was an effect of the high frequency envelope. The couplings shown in the figure started approximately 0.5 seconds after the onset of the first stimulus, reached a plateau after 1 to 2 seconds, and vanished within 150 msec afterwards. It is to be noted that the 40 msec correlation lag was the lag that maximized area A to area B coupling. Brun and Eckhorn did not report for what lag area B to area A correlation was maximized nor what the corresponding data looked like at this lag.

Several comments, not discussed in [48], are in order. First, distances between coupled regions in figure 18, based on the electrode placement shown in figure 16, are on the order of 40 to 80 mm. If we assume a mean axon diameter of 1 micron in the white matter [62]-[63] and accepted values for the speed of action potential propagation in axonal fibers [64], then the average time to directly propagate a signal over these distances is on the order of about 7 to 14 msec. From figure 14, the transient time required to establish a low-frequency change in membrane potential appears to be on the order of about 5 to 10 msec. Therefore the 40 msec lag reported in [48] has on the order of more than 10 msec of delay unaccounted for by these effects. It may, of course, be the case that the axonal route in the white matter is significantly longer than the direct distance between electrodes and that this extra distance is responsible for the unaccounted-for delay. However, it is also possible that the excess delay is indicative of polysynaptic connection between the regions, i.e. that the signal pathway is not a direct-coupled pathway. Allowing an average of about 1 msec for synaptic delay (action potential to evoked firing response), the number of intervening synapses most likely cannot exceed 10 to at most 28 synapses and it is probable that the actual number is below this range. This will have bearing when we discuss coupled oscillator models.

Second, although the data in figure 18 does show some correlation, one should not lose sight of the fact that most of these correlations are in a very low range. Bruns and Eckhorn did show that the *changes* in correlation were significant, but it is at the same time clear that other factors are intervening in the low-frequency-signal response beyond what is suggested by figure 15. It is not possible to infer from the results provided by [48] what these other factors may be.

Third, what is the implication of these results for Damasio's hypothesis (figure 11)? The presence of gamma-band ELFS correlation from region A to region B with the accompanying absence of such correlations from region B to region A could be interpreted as implying the absence of retroactive feedback from B to A. This would tend to contradict the convergence zone hypothesis. However, there are other possible interpretations that cannot be ruled out. It might be

that region B contains no convergence zones but that such convergence zones exist elsewhere, perhaps intermediate to regions A and B and acting retroactively on A while feeding forward to B. Bruns and Eckhorn noted with some surprise that area A showed no spectral amplitude responses to visual stimulation whereas area B did show them. This was surprising because area A was identified as early visual cortex, whereas area B was identified as belonging to the visual association area. Because area A was not unresponsive to visual stimuli, this can be interpreted to mean that gamma-band activity in area A is not stimulus-locked. This would imply either a strong local dynamic within functional columns of A, such that gamma-band firing activity is stimulated by but not locked to sensory afferents, or that gamma-band activity in area A is driven by retroactive feedback from some downstream convergence zone and the local firing activity is locked to this retroactive feedback. Neither possibility is ruled out by the data in [48]. It might also be the case that retroactive feedback from a convergence zone is not gamma- but rather beta-band signaling. Figure 18 and its time lag were chosen on the basis of maximizing the cross-correlation in area A to area B ELFS coupling. It was noted in [48] that the strong asymmetry between A-to-B coupling vs. B-to-A coupling applied only to the gamma frequency band. Perhaps the main B-to-A coupling is to be found at a different correlation lag and/or in a different frequency band. This, too, cannot be ruled out by the findings as reported in [48].

Finally, the data presented in [48] does not speak to whether or not any wave structure is implicated by the correlated couplings. The presence of a time lag in the ELFS correlation and more particularly the long persistence of the dwell in correlation (150 msec) after the ELFS correlation reaches a plateau suggests some form of signal propagation within the neocortex. Eckhorn et al. report that gamma wave propagation in the monkey visual cortex is very slow, on the average about 0.25 m/sec [58] vs. the 6 m/sec axonal propagation velocity we used earlier. Thus “gamma wave velocity” would be reflective of neuronal assembly dynamics rather than spike propagation via axonal transmission. We can note that a similar velocity, were it present in the neocortex of the experimental subject of [48], would implicate an ELFS lag of more than 160 msec, rather than the 40 msec found experimentally, if the change in the low frequency signal coincided with the onset or cessation of gamma-band oscillations at the destination.

VI. Oscillator Models of Synchrony, and Wave Propagation

VI A. Mathematical analysis of the preceding results. To put the results of the previous section into perspective with the various mathematical models that have been put forth, we need to take a look at mathematical correlation. Because any periodic signal can be expressed as a sum of sinusoids (Fourier’s theorem), it will suffice to consider two sinusoidal signals

$$x(t) = A_x \cos(\omega_x t + \theta), \quad y(t) = A_y \cos(\omega_y t) \ .$$

The cross-correlation function between x and y is defined as

$$R_{xy}(\tau) = \lim_{T\to\infty} \frac{1}{T} \int_{-T/2}^{T/2} x(t)\, y(t+\tau)\, dt \ . \tag{1}$$

If $\omega_x \neq \omega_y$ it is easily shown that $R_{xy} = 0$ for all values of τ. Thus, sinusoids at different frequencies are uncorrelated. If $\omega_x = \omega_y = \omega_o$, (1) becomes

$$R_{xy}(\tau) = \frac{A_x A_y}{2} \cos(\omega_o \tau - \theta) \ . \tag{2}$$

The correlation coefficient ρ_{xy} is the cross-correlation normalized by the geometric mean of the signal powers, i.e.,

$$\rho_{xy}(\tau) = \cos(\omega_o \tau - \theta) \tag{3}$$

and has a maximum value of ± 1 at lags

$$\tau = \frac{k\pi + \theta}{\omega_o}$$

where k is any integer. $\rho_{xy} = +1$ when k is even and -1 when k is odd. When x and y are composed of harmonic sums of sinusoids ρ_{xy} in general will have a maximum magnitude less than or equal to 1. An analytic expression for the lags at which the extrema of ρ_{xy} occur is unattainable in general. An exception occurs for the special case when $y(t) = x(t - T_D)$, in which case the maximum value of ρ_{xy} is equal to 1 and occurs at $\tau = T_D$.

We are now in a position to better understand the low correlation values reported in [48]. The lag used in the plots in figure 18 was selected to maximize the overall A-to-B ELFS correlations according to a complicated statistical sampling process described in [48]. Therefore the data in figure 18 does not correspond to a classical normalized cross-correlation function (which would have netted a zero value because the signals being correlated were in different frequency bands). Furthermore, the lag times evaluated in this process were sampled, i.e. trial values were reported as τ = 0, ± 10, ± 20, . . ., ± 100 msec. In addition, the bandwidths for the alpha-, beta-, and gamma-bands were relatively wide. It is therefore not surprising that low correlation values for envelope-to-envelope comparisons resulted; it is not statistically likely that the trial lag values would be such to maximize ρ_{xy} even if the time dispersion effect assumed in figure 15 were absent. Also, the test range for lag is less than what is necessary to detect slow gamma waves.

For example, suppose we have two signals

$$x(t) = \cos(\omega_o t + \theta) + \cos(2\omega_o t + \theta), \quad y(t) = \cos(\omega_o t) + \cos(2\omega_o t) \ . \tag{4}$$

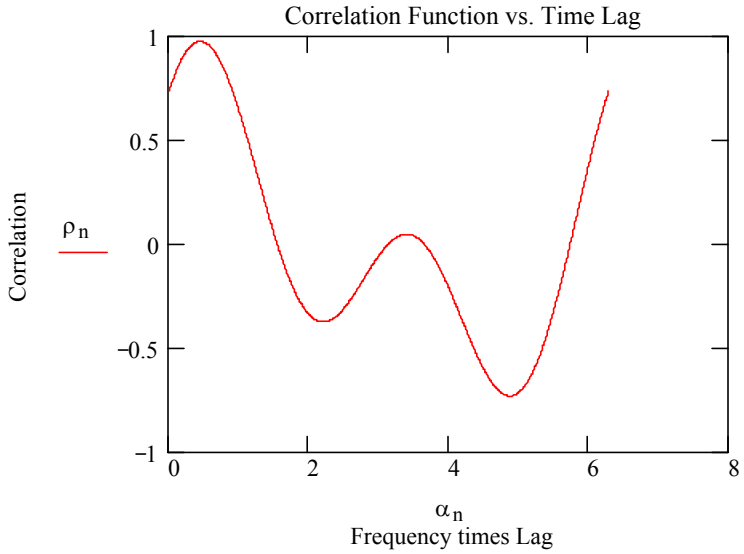

Figure 19: Plot of correlation coefficient for x and y functions of (4) with $\theta = 0.75$ rad. The parametric axis is $\omega_o \tau$ running from 0 to 2π radians.

The correlation coefficient $\rho_{xy}(\tau)$ is plotted for $\theta = 0.75$ as a function of $\omega_o \tau$ in figure 19. At a frequency of 25 Hz (edge of the gamma band), this plot corresponds to a 40 msec period, thus it is very unlikely that lags quantized to 10 msec steps would pick up the largest values of correlation coefficient. We can note that this function is less than 0.5 in magnitude over most of the range. This statement holds true for all values of θ, which primarily effects the magnitudes and locations of the extrema in the graph.

The low correlation coefficients in the envelope-to-envelope correlations in figure 17 therefore do not implicate the absence of alpha-, beta-, or gamma-band signals in comparing two regions, although they probably do indicate some amount of temporal dispersion is taking place. Most particularly, the low correlation coefficients do not unequivocally tell us that phase-locking is absent in any of the three bands. However, they do appear tell us that standing wave patterns are absent. To see this, we apply the standing wave equation given earlier and set

$$x(t) = \cos(\omega_o t), \quad y(t) = \sin(kd)\cos(\omega_o t).$$

where $k = 2\pi / \lambda$ and d is a distance from a standing wave node. Applying (1) and normalizing we obtain

$$\rho_{xy}(\tau) = \cos(\omega_o \tau). \tag{5}$$

Note that this result is independent of d. It is possible to choose sampled values for τ that produce small correlation coefficients even in the case of a standing wave. However, because a cosine function exceeds 0.5 in magnitude for 2/3 of its cycle and is maximal at zero lag, the

results from [48] are very likely to indicate the absence of *stable* inter-regional single-frequency standing waves in all three frequency bands (figure 17, coherence and phase consistency plots). Unstable standing waves (i.e. standing wave behavior established over only a short time period and then becoming disestablished) are not ruled out by the data presented in [48] since the authors noted that transient event-related coupling changes in areas A and B of about 500 msec duration did occur. They did not comment on inter-regional transient coupling, but they did imply that this phenomenon was not observed in the experiment. If no such transients occurred (as opposed to merely having gone unobserved), the experimental evidence of [48] would appear to rule out inter-regional single-frequency standing wave coupling.

However, the same argument *also* rules out the presence of stable inter-regional constant-velocity *traveling* waves. If we apply either of the traveling wave expressions given earlier and evaluate the correlation coefficient, we again obtain equation (5). When we consider the significant body of other experimental findings that conclude in favor of the traveling wave interpretation, this is a very strange and inconsistent mathematical finding. If no traveling waves are present, it is difficult to see how different cortical regions could synchronously communicate with each other at all, nor would a hypothesis that inter-regional binding codes are based on stable phase-coherent traveling wavefronts be supported. If traveling waves are merely transiently present, this would imply that wave-based binding codes could exist but are likewise transient in nature. However, such an interpretation would also imply that inter-regional transients, similar to the transient changes in the A and B regions noted by Bruns and Eckhorn in [48], should have been present. Traveling waves with non-constant velocity ('lurching waves') are not ruled out.

The analysis does not rule out yet another possibility. It might be that functional columns or hypercolumns (assemblies of linked functional columns) in different regions establish locally synchronous firing patterns but do so at different frequencies from one region to another or in response to a stimulating input activity characterized by a different frequency (stimulated oscillation). In this hypothesis, transient traveling waves might merely stimulate firing activity in other remote regions but different regions would be neither phase- nor frequency-locked. Something similar to this has been proposed by Eckhorn [37].

This does, of course, immediately raise the question of what physical variable is to be looked upon as the representation of a neural code. What can be said at this point is that such a variable could be neither a particular single frequency nor a single phase or phase delay measure. It also raises the question of what precisely constitutes the "coupling" variable or parameter between regions that "holds the object representation together" if neither synchrony nor phaselock nor wave coherence nor phase continuity can stand by itself as the mechanism for longer-term

binding. It is clear that fast, synchronous *local* oscillations are characteristic of neuronal activity in object representation [37], and it is clear that fast synchronous firing activity is not maintained between different spatial regions of the cortex [48].

VI B. Coupled Oscillator Models of Cortical Synchrony. With all this in mind, let us now examine the various mathematical models that theorists have put forth in pursuit of cracking the neural code. The principal goal of most mathematical theorists in this field of study is not so much to attain to an understanding of cortical function as it is to bring to light the characteristic properties of various mathematical functions so as to understand what can and cannot be explained on the basis of different mathematical models. All the dynamics involved in these kinds of systems are highly nonlinear, few have closed-form solutions, and all have dynamical properties that are crucially dependent upon modeling parameters. It can be fairly stated that the endeavors of the mathematicians are aimed at helping to carry the state of our knowledge from the realm of the purely phenomenological closer to the realm of the theoretical. More specifically, the work is directed toward understanding the collective behavior of a large assembly of interconnected elements ('cells'). Thus, all the mathematical studies that have been carried out are based on greatly simplified systems, typically one- or two-dimensional coupled chains or arrays of oscillators or 'neurons', based on greatly simplified models of neuronal oscillation.

The Kuramoto Model. An early example of the assembly-of-oscillators approach to modeling is the Kuramoto model [65]-[68]. This model was not aimed specifically at modeling the cortex, but it has nonetheless stimulated a great deal of modeling work in theoretical neuroscience. We will only briefly describe this model and touch upon certain highlights of it. A fuller tutorial on the mathematics of the Kuramoto model is provided in [69].

The Kuramoto model considers a fully interconnected assembly of N identical oscillators. Each oscillator, n, is described by a phase variable, ϕ_n , and a parametric constant ω_n called its eigenfrequency. The system is described by a set of N coupled first-order differential equations

$$\dot{\phi}_n \equiv \frac{d\phi_n}{dt} = \omega_n - \frac{K}{N}\sum_{j=1}^{N}\sin\left(\phi_n - \phi_j\right) \tag{6}$$

where K is a coupling constant characteristic of the assembly. In the language of system theory, the quantity $\dot{\phi}_n$ is called the **instantaneous frequency** of oscillator n.

It is obvious that a Kuramoto oscillator is not a model of a "neuron" because it is essentially merely an oscillator. It does not "spike" (produce action potentials), although if one wished one

could adopt the convention that a "spike" is represented when ϕ takes on values very close to zero or π or some other chosen value. But at best it can only be viewed as a highly abstracted model of neuronal behavior. It is closer to the spirit of the model to say that each oscillator represents the collective behavior of a single functional column or hypercolumn of neurons. Even here, however, there is a serious restriction because each oscillator has only a single eigenfrequency, whereas we have seen that functional columns in the neocortex exhibit multiple co-existing firing rates. Furthermore, each Kuramoto oscillator affects all the others for all values of ϕ_n , whereas neurons can affect one another only when they spike.

If all one wishes to do is to simulate the behavior of the system, one merely runs a numerical solution for the system given by (6) from some set of initial conditions. However, this is not what the mathematicians are after. Rather, the goal is to understand fundamental properties of systems that are described by the set of equations (6). To do so, the system is *analyzed* by introducing a function that system theorists call a Lyapunov function, and which physicists frequently call a Hamiltonian. In physics a Hamiltonian is the sum of the kinetic and potential energies of the system, and a stable solution is one for which the Hamiltonian function is minimized. Thus, to analyze the solution of (6) we must find a Lyapunov function and minimize it with respect to the phase variables. This is done by introducing the average eigenfrequency of the system

$$\Omega = \frac{1}{N}\sum_{n=1}^{N}\omega_n$$

and making a change of variables

$$\varphi_n = \phi_n - \Omega\, t \ .$$

With these, the derivation of the Lyapunov function is straightforward and the result is

$$\mathcal{H} = -\frac{K}{2N}\sum_{n=1}^{N}\sum_{m=1}^{N}\cos(\varphi_n - \varphi_m) - \sum_{n=1}^{N}(\omega_n - \Omega)\varphi_n \ . \qquad (7)$$

The details of the derivation and the details of the analysis of the conditions under which (7) is minimized are presented in [69] and we will not go into them here. Rather, we will summarize the principal findings. The first of these is that a phase-locked state, i.e. $\dot{\phi}_n = \dot{\phi} \ \forall\ n$, is a minimum of $\mathcal{H}$. Furthermore, there is a critical value for coupling, K_c such that for $K > K_c$ the system phase-locks. In this state every oscillator oscillates at the same instantaneous frequency. If $K < K_c$ no phase-locked solution exists. The critical value depends on the spread between values of the eigenfrequency parameters ω_n. If K is below the critical value but the spread in eigenfrequencies is not too great, there may be partial phase-locking, i.e. some of the oscillators will phase-lock with each other but not all of them will do so. The oscillators having values of ω_n at the extremes

of the distribution will not phase-lock with the rest of the assembly. There is another critical value, $K_{pc} < K_c$, such that if $K < K_{pc}$ no partial phase-locking takes place and the entire assembly behaves incoherently.

As a model of the neocortex, the Kuramoto model has some very obvious flaws. First, every oscillator cell is coupled to every other cell with the same coupling coefficient. Second, there are no inputs. Third, every cell always oscillates; there is no mechanism for any part of the network to 'go silent.' These are very serious shortcomings when it comes to using Kuramoto's system as a model of neocortex.

The Schuster-Wagner Model. Some of these issues are overcome by the Schuster-Wagner model [70]. In this model a **column** is defined as a collection of N_e excitatory neurons and N_i inhibitory neurons which are globally coupled. Each neuron is described by the **firing rate model**, i.e. each neuron k is characterized by the rate , e_k or i_k, at which it fires action potentials in response to its input p_k. Each column is described by the average firing rate E of its excitatory neurons and the average firing rate I of its inhibitory neurons. This is a **population model** because we ignore the details of the individual neurons in a column and focus instead only on the average behavior of the column. The system is made up of interconnected columns. This is illustrated for the case of a two-column system in figure 20 [69].

The mathematical details are, naturally, more involved than those of the Kuramoto model. However, the analysis shows that for each column there is a range of input firing rates

$$P_{cl} < P < P_{ch}$$

such that for reasonable parametric values the column solution is oscillatory. Outside this range we have fixed-point (i.e., non-oscillatory) solutions. With N coupled columns (e.g. figure 20b) the

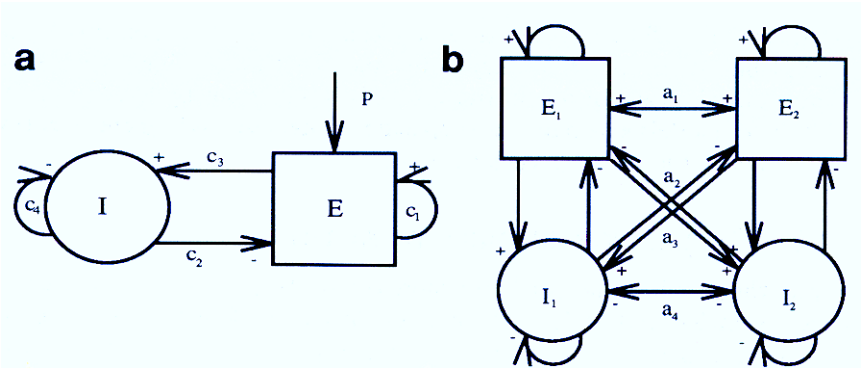

Figure 20: Schuster-Wagner population model. Each column is composed of an excitatory intra-column E and an inhibitor intra-column I (a). Intra-columns are interconnected as shown in (b). Inputs are applied only to the excitatory intra-columns. Excitatory couplings are marked with a +; inhibitory couplings are marked with a – . Each column n is characterized by a phase variable ϕ_n.

system dynamics are described approximately by a set of N coupled equations

$$\dot{\phi}_n = \omega(P_n) - \sum_{j=1}^{N} J_{nj} \sin(\phi_n - \phi_j)$$

where $\omega(P_n) = \omega_n$, an eigenfrequency, if column n is active and zero otherwise. $J_{nj} = K$ if both columns n and j are active and zero otherwise. This of course is nothing other than a Kuramoto model insofar as the active columns are concerned. For the inactive columns $\dot{\phi}_n = 0$. A column is active if its input $P_n > P_{cl}$. The phases ϕ_n in this model, because they represent some kind of average population behavior in a column, are fictitious in the sense that they cannot be interpreted as individual neuron behaviors. There are other interpretational difficulties with this model and the many derivatives of it. Some of these details are described in [69].

Wang's Model. Wang's model [71] is in some ways similar to the Schuster-Wagner model, but it takes its starting point from an earlier model by Wilson and Cowan [72]. The basic unit is an oscillator made up of one excitatory and one inhibitory 'neuron.' The signal quantities in the model are 'activities,' which represent mean firing rates [72], [6, pp. 103-112]. For the i^{th} oscillator x_i represents the activity of the excitatory 'neuron' and y_i denotes the activity of the inhibitory 'neuron.' The excitatory 'neuron' is allowed to receive external stimuli I_i , which is interpreted as the mean firing rate of external inputs, and is allowed to receive inputs S_i from other excitatory 'neurons.' There are various possible functions for representing S_i [6], the most commonly encountered of which is a weighted sum $S_i = W_i^T X$ where W_i is a vector of interconnection weights and X is a vector of activities for all the excitatory neurons in the system. Each excitatory neuron is also presumed to be semi-stochastic inasmuch as it is given an internal Gaussian 'noise' term of mean amplitude ρ. Each Wang oscillator is described by the set of equations

$$\begin{aligned} \frac{dx_i}{dt} &= -x_i + G_x[x_i - \beta y_i + S_i + I_i + \rho] \\ \frac{dy_i}{dt} &= -\gamma y_i + G_y[\alpha x_i] \\ G_r(\nu) &= \frac{1}{1 + \exp(-(\nu - \theta_r)/T)}, \quad r \in \{x, y\} \end{aligned} \qquad .$$

Here α and β are positive coupling terms, γ is a positive decay term, θ_r (r = either x or y) is a threshold constant, and T is a parameter that controls the firing rate in response to the argument of the sigmoid function G_r . The Wang oscillator and an example of a one-dimensional oscillator chain is shown in figure 21.

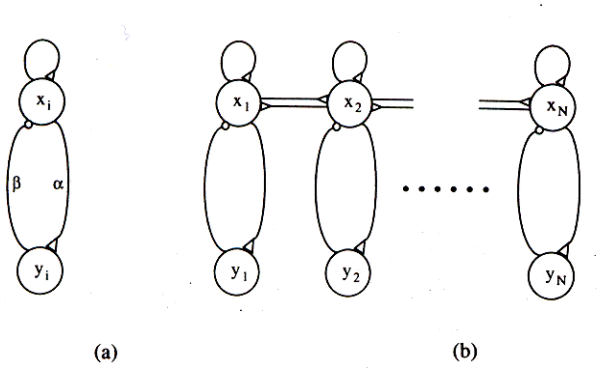

Figure 21: Basic Wang oscillator (a) and an example of a one-dimensional chain of oscillators (b).

The oscillator model belongs to that class of systems said to be 'mean field approximations' of neural network activity. Wang presented simulation results but no detailed mathematical analysis in [71]. He did, however, point out two characteristics of systems such as that of figure 21b that are interesting and of wide application. First, weak coupling (e.g., small values in the *W* vectors) does not disrupt the oscillatory behavior of individual oscillator cells. He did not quantify 'weak.' Second, he proposed that so long as the sum of the weights of all connections converging on every oscillator from all other *active* oscillators is kept constant, phase-locking occurs among these oscillators. Wang calls this the **equal weight condition**. Because oscillators are not necessarily active, dynamical changes in the network must be accompanied by dynamical changes in the weights of the connections among 'neurons' if synchrony and phase-locking is to be achieved. This requires rapid modulation of connection weight values, an idea which was first proposed by von der Malsburg in [22]. Neural network models based on such fast elastic weight modulation have since come to be known as **dynamic link architectures** (DLAs) [73]-[75].

Another important contribution of the Wang model is that it was demonstrated to be capable of producing synchrony using only local connections (whereas the Kuramoto-type models required the network to be globally connected in order to achieve synchrony). This is important because globally connected networks cannot segment themselves, which is an important computational ability for neural networks since segmentation of inputs is a key requirement for discriminating among different perceptual objects. Although Wang was primarily interested in networks that could achieve synchrony (phase-locking with zero phase difference), he also reported that some arrangements of interconnection weights produced phase shifts in activity across the oscillator chain.

Other Oscillator-Network Models. We have so far looked at network models based on phase-model oscillators (Kuramoto model and its derivatives) and firing-rate models. A criticism

sometimes leveled against these models is that they are too phenomenological. Why should we think that the properties of such models have anything to do with the property of biological neural networks? Would we not be on firmer ground if our oscillators were derived from known properties of biological neurons? This brings us to oscillator network models whose oscillators are patterned after biological dynamics.

The starting point for "biologically realistic" oscillator models is usually grounded in the work of Hodgkin and Huxley in 1952 [76]. The Hodgkin-Huxley (H-H) model of the physiology of action potential generation in the giant axon of the squid (for which they won the Nobel prize) consists of a set of coupled nonlinear first order differential equations. Hodgkin-Huxley style models extended to the neuron as a whole, e.g. [77]-[78], or to its dendrites and soma compartmentally, e.g. [79], have been the foundation of physiological neurodynamics ever since. Unfortunately, the computational complexity of H-H models usually limits them to neural networks involving only a few neurons. With biologically reasonable parameter values it is often possible to approximate H-H dynamics using a reduced set of simplified equations. Probably the first such model was the FitzHugh-Nagumo (F-N) model [80], [81, pp. 71+]. Another such model due to Morris and Lecar (M-L model) has also been popular among theoreticians [20], [6, pp.153+]. The Wilson models shown earlier [4] are yet another such example.

However, even these models are too computationally expensive to use in small neural networks comprised of a few hundred neurons. For this reason network theoreticians make additional simplifications to these equations. The Terman-Wang oscillator (T-W) model [82] is a derivative of the M-L model. Campbell et al. have shown the T-W model can be used to describe a variety of four different types of relaxation oscillators, including sinusoidal, square-wave, spiking, and a class they call 'singular limit' oscillators [83]. The T-W oscillator is described in terms of two state variables

$$\frac{dx}{dt} = 3x - x^3 - y$$
$$\frac{dy}{dt} = \varepsilon\left(\lambda + \gamma \tanh\left(\beta x\right) - y\right)$$

where the various terms in the equations are constants that determine the dynamical properties of the oscillator. Coupled oscillator networks are formed by adding terms to the equation for the derivative of x. These terms are functions of the x terms of the other oscillators, usually in the form of a sigmoid function [83], e.g. G_r in the Wang model equations above.

Campbell et al. presented numerical results for various types of oscillator chains in [83]. From these they empirically characterized synchronization rates. Although they present no formal proofs or results, they did present some interesting qualitative findings. First, the solutions they

obtained were always synchronous solutions rather than solutions with relative phase delays (when any such solution existed). Not surprisingly, they found that the form of the interaction between oscillators was an important factor in determining the synchronization rate. Like many other investigators, they found that the system dynamics exhibited both a fast-time-scale and a slow-time-scale mode. In chains of relaxation oscillators (a class that includes F-N oscillator models) the coupling strength between oscillators must be above some critical threshold or else initial-condition-dependent non-synchronous as well as initial-condition-dependent synchronous solutions are possible. In general they found that chains of relaxation oscillators achieved synchrony at a faster rate than spike oscillator chains. They claimed that chains of relaxation oscillators can form "clusters" of synchronous oscillators, a finding that extends a previous finding they had made on chains on spike oscillators [84]. Perhaps most interesting, they make the conjecture that in a one-dimensional chain of identical relaxation oscillators traveling wave solutions are not possible unless the chain forms a ring and then only under very particular topological conditions [85]. Similarly, they reported that traveling wave solutions in two-dimensional arrays could occur under periodic boundary conditions (the two-dimensional counterpart of the one-dimensional ring of oscillators), and that rotating wave solutions were also possible. In both cases, however, the production of a traveling or a rotating wave was initial-condition dependent. While their conjecture is not proven, it is widely acknowledged by many experts as likely being true.

The findings presented by Campbell et al. in [83] are empirical. Medvedev and Kopell have presented us with some formal mathematical findings on the properties of coupled relaxation oscillators of the FitzHugh-Nagumo class [86]. They studied chains of F-N oscillators in the limit of strong coupling with a gradient in the eigenfrequencies of the successive oscillators. In general the relaxation oscillator is described by a pair of state variables, here denoted as v and u. One of these (v) is regarded as analogous to neuron membrane potential and the other (u) is regarded as analogous to some internal dynamical variable. In the case of [86] u was regarded as analogous to intracellular concentration of Ca^{2+}, which affects membrane potential through the mechanism of Ca^{2+}-dependant potassium ion channels in the neuron. (K^+ channels generally provide for hyperpolarization of the neuron). The relaxation oscillator equations are

$$\varepsilon \frac{dv_i}{dt} = f(v_i) - u_i$$
$$\frac{du_i}{dt} = \omega_i (v_i - \kappa u_i)$$

where ε and κ are some (usually small) positive constants and $f(v)$ is a qualitatively cubic-like

function, e.g. $f(v) = v(1 - v^2)$ or some other piece-wise continuous function that has the same general shape ($f(0) = 0$, one negative minima, one positive maxima). Medvedev and Kopell set $\kappa = 0$ and studied strongly coupled FitzHugh-Nagumo oscillator chains of the form

$$\varepsilon \frac{dv_1}{dt} = f(v_1) - u_1 + d \cdot (v_2 - v_1)$$
$$\varepsilon \frac{dv_i}{dt} = f(v_i) - u_i + d \cdot (v_{i+1} - 2v_i + v_{i-1}), \quad i = 2, 3, \cdots, N-1$$
$$\varepsilon \frac{dv_N}{dt} = f(v_N) - u_N - d \cdot (v_N - v_{N-1})$$
$$\frac{du_i}{dt} = \omega_i v_i, \quad i = 1, 2, \cdots, N$$

where $d >> 1$ is the coupling constant. They noted that their main results generalize to the case where the coupling constants are different between nearest-neighbor pairs in the chain provided the constraint on d is still met. Their analysis assumed $\omega_1 < \omega_2 < \ldots < \omega_N$.

The system described by the above set of equations is describable by a 2N-dimensional phase space. By means of an elegant perturbation analysis using a Lyapunov function, they achieved the following main results. In the large coupling limit the phase space contains an N – 1 dimensional cylinder. Phase trajectories rapidly approach this cylinder (a 'fast' time scale) and then slowly drift along it toward a unique limit cycle oscillation. The transient time required to reach the stable limit cycle is inversely proportional to d; therefore transients are longer for stronger coupling. They demonstrated that a synchronous solution exists and that, to an approximation of zeroth order, the synchronous oscillation frequency is the mean-value of the eigenfrequencies of the system. They further showed that the coupled variables v_i quickly become practically indistinguishable but that the internal variables u_i differ from cell to cell, although in all cases u_i remains synchronous with v_i. The slow transient shows up most markedly in the u_i variables. They also made the surprising finding that the conclusions of the paper do not necessarily hold if κ is made non-zero, even if it is small. In particular, the dynamics of u_i are very sensitive to the value of κ. For magnitudes of κ less than $1/(2d)$ the system still asymptotically approaches a limit cycle at a rate inversely proportional to d, but for positive κ magnitudes above this value the rate of convergence becomes faster and dependent on the value of κ. For negative κ with magnitude greater than the critical value periodic solutions vanish. Because d is large, the critical value is very small. This result is surprising because it has often been assumed that coupled F-N systems would not be very sensitive to small values of κ.

General Synopsis of Coupled Oscillator Models. We have briefly looked at two extreme cases of

coupled-oscillator networks. We can summarize the general properties as follows [87]. Because the details of the neural networks that form oscillators are often not known, the aim of the mathematical analysis of coupled oscillator systems is to find the consequences of what is known about such systems and to generate well-defined questions for the experimenter to answer. When the system is weakly coupled it is possible to obtain a well-defined phase for each oscillator and then the coupling between oscillators only depends upon phase differences. The general form for such a system can be written as

$$\frac{d\theta_j}{dt} = \omega_j + \sum_k H_{jk}\left(\theta_k - \theta_j\right) \tag{8}$$

where H_{jk} is some function that describes how much oscillator j speeds up or slows down as a consequence of interaction with other oscillators k. This function is obtained by averaging the effects of coupling terms from an original, and more biologically fundamental, model of the neural system, the average being taken over one cycle. H will depend upon the properties of the biological oscillators as well as on the nature of the inter-neural coupling between oscillators. When it is possible to find a coupling function H by means of averaging methods (which is not always possible and appears to always require weak coupling), the resulting model is called a phase model.

If the coupling in a phase model is too weak, neither synchrony nor wave solutions result. Under some conditions a coupled phase model is capable of producing waves. The simplest case is that of nearest-neighbor coupling, in which case (8) can be re-expressed as

$$\frac{d\theta_j}{dt} = \omega_j + H_A\left(\theta_{j+1} - \theta_j\right) + H_D\left(\theta_{j-1} - \theta_j\right) \tag{9}$$

where H_A is the coupling function in the ascending (caudal to rostral) direction of the chain and H_D is the coupling function in the descending (rostral to caudal) direction in the chain. There are at least three mechanisms in such a system for producing traveling waves.

1. Eigenfrequency gradient: When the eigenfrequencies ω_i are unequal and change monotonically in one direction, e.g. $\omega_1 < \omega_2 < \ldots < \omega_N$ or vice versa, a traveling wave propagating from the higher to the lower eigenfrequency is produced. However, the phase lags are not constant (i.e. are position-dependent) and so here we do not have a classical traveling wave of the form $u(\beta x - \omega t)$ [88]. Rather, the wave velocity is non-constant.

2. One-way coupling: When the coupling in (9) is one-way (e.g. $H_D = 0$) and the eigenfrequencies are equal the oscillators will lock with a non-zero constant phase difference for some choices of H_A. For example the coupling function

$$H_A(\varphi) = \alpha\sin(\varphi) + \beta\cos(\varphi), \quad \beta \neq 0$$

has been shown to support traveling waves of this sort.

3. Gradient in coupling strength: Traveling waves can also be produced if there is a gradient in coupling strength, i.e.,

$$\frac{d\theta_j}{dt} = \omega_j + s_j H_A\left(\theta_{j+1} - \theta_j\right) + s_j H_D\left(\theta_{j-1} - \theta_j\right)$$

where s_j varies monotonically with j.

In all cases, if the eigenfrequencies are unequal the wave speed is not constant along the chain. One very interesting finding that has been made is that if the chain described by (9) is very long but still finite, these two-way-coupled oscillators behave like a chain with only one-way coupling provided that the two-way coupling is asymmetric ($H_A \neq H_D$). The reason is because in these cases one of the directions dominates the other. The non-dominant coupling affects only the phase lag near one end of the chain. Here a 'boundary layer' is established in which the phase lags differ from the rest of the chain. However, this only happens in long chains because for short chains the boundary layer may take up most of the length of the chain.

When we extend (9) to the case of coupling among non-nearest neighbors, but still restrict the coupling distance to be a small fraction of the length of the entire chain, many of these same results are still obtained. However, the mathematics shows that the phase lags are decreased [89]. There has not been a great deal of study involving long-range coupling. It has been demonstrated that when there is long-range coupling from the ends to an interior region of a chain and when this coupling is anti-phase (opposite phase) between the oscillators that are directly coupled then both traveling waves or standing waves can be produced [90].

When we turn to the case where we have strong coupling or when the H function cannot be obtained through the averaging approach mentioned earlier, the situation is very different. With stronger coupling we generally cannot identify a local phase for each oscillator, and likewise when the coupling function cannot be expressed as in (8) then even if we have a locally-definable phase the coupling interaction is not described in terms of simple phase differences. This is the regime where relaxation oscillator models are usually employed. In general it is very difficult to obtain traveling wave solutions in this regime, and if the Medvedev-Kopell conjecture is true it is impossible. The usual outcome is synchrony with phase lags very close to zero among the oscillators. Long chains of relaxation oscillators can lock to each other within a few cycles, although they may take a long time to reach a steady-state limit cycle of oscillation. Chains described by (8), on the other hand, can take a long time to lock with each other when the coupling strength is large enough to produce synchrony rather than traveling wave solutions. As

we saw in the case of the Wang oscillator network, it appears to be the case that synchrony requires something like the equal-weight condition (that is, there has to be short-term dynamic link modulations). Furthermore, dynamic link modulation appears to be necessary if the oscillator network is to be able to support segmentation of different input patterns because otherwise the entire network phase-locks in synchrony (which prevents us from being able to distinguish different object patterns from one another).

VII. Spiking Models of Wave Propagation

Although synchrony is experimentally observed in cortical systems, it has also been found that such synchrony does not extend past more than just a few millimeters of cortex. It is therefore evident that cortical organization cannot consist of nothing but chains of strongly-coupled oscillators. We have likewise argued that the experimental findings from [48] suggest that even constant-velocity traveling or standing waves are unlikely. Consequently, a pure phase-oscillator model of region-to-region coupling appears to be inadequate for describing real cortical systems. Let us therefore turn our attention to models in which the local cells are not inherently oscillatory. For this we turn to spiking neuron models and the behavior of networks comprised of them.

VIIA: LIF and Theta Networks

Neuron models intended for use in large network simulations must as a practical matter be simple. There are several such simple models derived as limiting cases of more biologically realistic models. The oldest and simplest of these is the leaky integrate-and-fire model (LIF) [81, pp. 94-97]. Another simple canonical model is the "theta" model introduced by Ermentrout and Kopell [91], [92, pp. 118-123]. The LIF and theta models, despite some prominent underlying differences in their mathematical formulation and in the interpretation of their state variables, give more or less similar performance in neural network models. The most prominent difference is that the theta model requires more computer time to run than does the LIF model [92].

Traveling waves have been demonstrated in both LIF networks [93]-[94] and theta-neuron networks [95]. Because the theta model incorporates more of the main qualitative features of the majority of mammalian neurons (i.e. distinct subthreshold and superthreshold regions, an all-or-nothing spike output, a steady-state resting point and a relative refractory period) we will review the theta neuron network results reported by Osan et al. [95]. They studied wave propagation in a one-dimensional chain of theta neurons in the absence of external inputs. Network activity was induced by setting one of the neurons to an initial condition above its firing threshold in order to start the wave. Their formal analysis was taken in the continuum limit with neurons coupled

through a symmetric coupling function $J(x)$ having the properties: 1) $J(x) = J(-x)$; 2) $J(x) \geq 0$; and 3) $dJ/dx < 0$ for $x > 0$ where x is the distance between neurons in the chain. The specific form for $J(x)$ employed in their explanation of method was

$$J(x) = g_{syn} e^{-a|x|}$$

where g_{syn} is the maximum coupling value and a is a space constant. The spike function employed was a simple decaying exponential.

The principal findings of [95] are the following. First, there is a lower bound on g_{syn}, below which traveling waves will not propagate in the network. (A similar result has elsewhere been found for LIF networks as well). Osan et al. give an expression for the lower bound. Second, in networks where wave propagation is possible, they proved that every neuron participating in the wave will spike more than once. Their analysis method did not allow them to determine the number of times a neuron would spike.

Figure 22 illustrates a simulation example of wave propagation in their network. The finding that multiple spikes are elicited from each neuron is conjectured to be a consequence of the absence of inhibition in the network. We can note the occurrence of multiple spikes from each neuron. Close examination of the figure in the upper right-hand corner shows that at roughly 130 msec the network begins to back-propagate as well as to forward-propagate waves. This is shown by the development of a C-shaped curvature in the space-time plot. Osan et al. did not comment on whether the wave behavior eventually died out or if the network continued to propagate waves

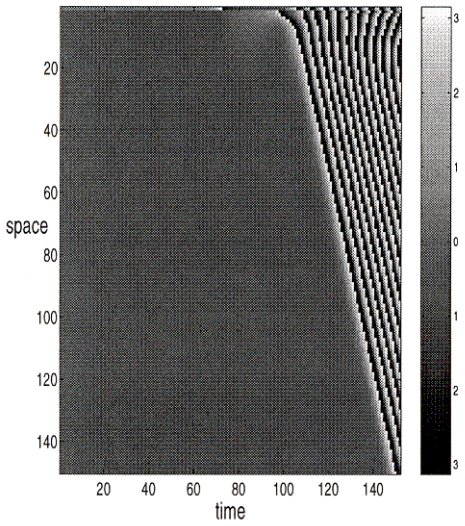

Figure 22: Simulated wave propagation in an excitatory one-dimensional chain of theta neurons [95]. The gray scale gives the value of the state variable of the theta neurons. Spiking occurs when the color of the cell is white. There were 150 neurons in the chain. Vertical position corresponds to the neuron locations.

once this behavior was initiated.

This last question is an important one. We might think that the one-dimensional chain is a rather arbitrary configuration, and we would naturally be inclined to ask if more complex networks might not show entirely different behavior. Here some insight can be gained from studies of randomly-connected networks in which small 'netlets' of neurons are directly coupled. One of the earliest of such studies was carried out by Annimos et al. in 1970 [96]. They studied networks based upon the simplest of all spiking neuron models, the McCulloch-Pitts or 'point' neuron [18, pp. 152-153]. Anninos et al. developed a probability expression for the expected percentage of neurons that would fire at the next time step in a large randomly-connected network given the percentage that were firing at the current time step and the number of excitatory inputs required to fire a neuron. Figure 23 illustrates their results for a family of curves based on the number of excitatory inputs required to fire a point neuron.

In figure 23 steady-state solutions are marked by the intersects between the curves and the line y = x. The zero firing state is one such intersect. In this figure, thresholds 4 – 7 have only this intersect. For threshold = 1 there are two stable solutions, zero and a high-rate firing point located

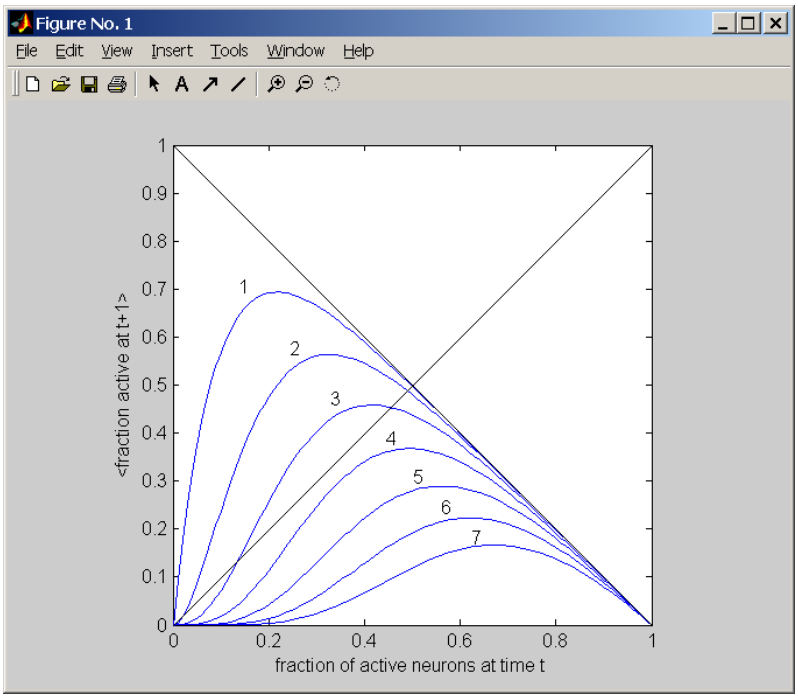

Figure 23: Fraction of active neurons at the next time step vs. number active at the present time step and number of excitatory inputs required to fire a neuron in a randomly-connected McCulloch-Pitts network. Firing thresholds are given above and to the left of each curve. The netlets consisted of 10 neurons each. The points where the curves intersect the y = x line going up and to the right is either a steady-state solution or an unstable 'ignition point'.

at approximately the 50% of the population. Thus for threshold T = 1 the only solutions are either the quiescent state or a state in which half the population is firing at any time step. For the T = 2 and T = 3 curves there are three intersects, corresponding to the zero point, an unstable 'ignition point' and a high firing population point. Therefore, these curves also have only the quiescent and high firing population points as steady-state solutions. Furthermore, it is known that adding inhibitory synapses merely shifts the family of curves and does not change this qualitative picture [18]. Note that for the thresholds T = 4 – 7 in figure 23 the population of firing neurons decreases monotonically to zero from whatever initial firing population condition is imposed. It has further been shown that a low but non-zero firing population in the steady-state in such a network is only obtained when the network is driven by an external input that forces a small but non-zero fraction of the population to fire [18].

High population activity percentages are not observed in the neocortex. Rather, only a small fraction of the neural population is firing at any particular moment in time, and a zero percent condition is never observed in a living organism. In general it appears to be quite difficult to obtain low but non-zero firing populations in randomly connected neural networks populated by non-oscillatory 'neuron' cells. This problem has also been studied by Pantiliat [97] and by Nelkon [98]-[99]. The source of the difficulty appears to be the extrasynaptic delay involved in firing inhibitory neurons in the network. For this reason it has been conjectured that in neocortex the delay in propagating a signal to excitatory neurons in other regions of the cortex must be greater than the delay in propagating signals to the inhibitory neurons. This conjecture is consistent with the cortical organization of functional columns, where the delay to local inhibitory interneurons is small compared to the delay in propagating signals via the white matter to remote cortical regions.

The significance of these findings for the model presented in [95] is the following. Although their network is not a 'random' network, and although it does not consist of McCulloch-Pitts neurons, it is a purely excitatory network. The existence of a minimum coupling constant as necessary for wave propagation to be produced from the firing of a single neuron implies that this network does possess the function equivalent to an 'ignition point'. The fact that figure 22 appears to approach a condition in which a sizable fraction, approaching one-half, of the neurons are firing is strongly similar to the T = 2 and 3 curves in figure 23. If it is true as conjectured here that the wave activity will not die out spontaneously, then combining the Anninos analysis with the findings of [95] implies that the network of [95] cannot be a realistic model of neocortical organization. Furthermore, the mere addition of inhibitory connections seems unlikely to produce wave behavior and a low percentage firing population in the same network, contrary to a

conjecture made in [95].

VIIB. The 'T-current' Network and Lurching Waves. Some excitatory neurons have the interesting property that they fire a pulse following the cessation of *inhibitory* inputs. This is indeed a relatively common phenomenon and it is sometimes called post-inhibitory rebound or PIR. PIR is conjectured to be the mechanism for some forms of central pattern generators (CPGs) in the spinal cord and the cerebral hemispheres. One physiological mechanism for PIR is the existence in some neurons of an inactivating voltage-dependent sodium current or a class of calcium currents known as T-currents [77]. At the normal resting potential these channels are inactivated. A hyperpolarization of the cell membrane removes the inactivation and, upon release from the hyperpolarizing input, the T-channel opens and can produce one or more action potential spikes before again inactivating. Rhythmic networks based on T-current dynamics have been found in the thalamus. Network models based on FitzHugh-Nagumo-like coupling and constructed to mimic the PIR dynamics have been reported by Rinzel et al. [100] and by Terman et al. [101]. The main difference between these chains of neurons and those of [95] is that signal propagation along the chain passes first through the equivalent of an inhibitory cell before reaching the equivalent of an excitatory cell, and that stimulation of the excitatory response is by PIR. Thus the problem confronting Anninos-like networks – i.e. the need for having shorter delays to inhibitory responses than to excitatory ones – is automatically satisfied in this model.

Terman et al. studied one-dimensional chains of the form

$$\frac{dv_i}{dt} = f\left(v_i, h_i\right) - \frac{g_{syn}}{N}\cdot\left(v_i - E_{syn}\right)\sum_{j=1}^{N} W_{ij}s_j$$

$$\frac{dh_i}{dt} = \varepsilon\cdot\left(h_\infty\left(v_i\right) - h_i\right)/\tau_h\left(v_i\right)$$

$$\frac{ds_i}{dt} = \alpha\cdot\left(1 - s_i\right)\cdot H\left(v_i - \theta\right) - \varepsilon\cdot\beta\cdot s_i$$

where H is the Heaviside step function, f is any function having a cubic-shaped nullcline, and

$$h_\infty\left(x\right) = \frac{1}{1+\exp\left[-\left(v-\theta\right)/\sigma\right]}, \quad \tau_h\left(x\right) = \tau_R + \frac{\tau_L - \tau_R}{1+\exp\left[-\left(x-\theta_{h\tau}\right)/\sigma_{h\tau}\right]}.$$

These latter two equations are sigmoid expressions for nonlinear membrane dynamics that produce the PIR effect. The synaptic weighting function W_{ij} was taken to be some function of the distance between neurons, i.e. $W_{ij} = W(i - j)$. This function is called the 'synaptic footprint' and two types were considered. If W is maximal at $W(0)$ the footprint is called ON-CENTER. If $W(0)$ is small or zero and the maximal coupling takes place for some non-zero $i - j$ the footprint is called OFF-CENTER. The neuron output signal is s_i and v_i and h_i are state variables of the

neuron. The other terms above are various constants provided in [101].

The principal findings of [101] are as follows. Two classes of traveling wave solution are found. The first, illustrated in figure 24, is the usual traveling wave with constant wave velocity, which they refer to as a smooth wave. The second, illustrated in figure 25, is a wave with non-constant propagation velocity. This wave, named a 'lurching wave' by Rinzel [100], 'jumps' from neuron to neuron with various time delays, somewhat resembling saltatory conduction of action potentials found in myelinated axons.

For smooth waves single-pulse, multiple-pulse, and periodic solutions were all found. Multiple bursting pulse solutions were among the multiple-pulse solutions. Their analysis showed that smooth wave solutions were not possible for ON-CENTER synaptic footprints without gaps. The production of smooth waves required an OFF-CENTER synaptic footprint. They provided an

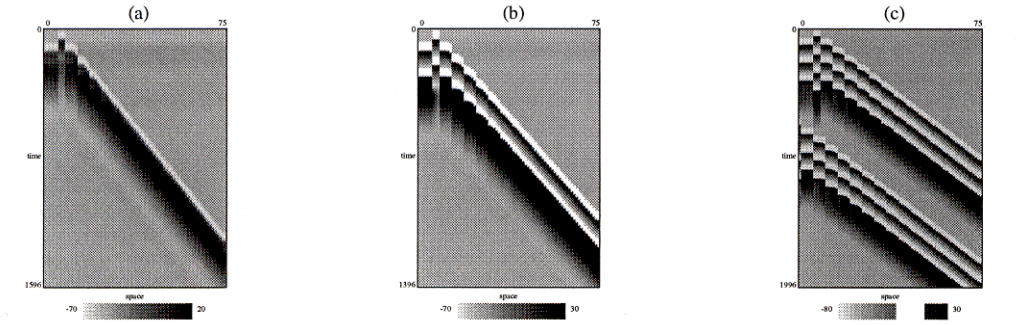

Figure 24: Smooth wave solutions found through simulation in [101]. Single-pulse, double-pulse, and periodic smooth wave solutions were found. (a) single-pulse solution; (b) double-pulse solution; (c) a multiple-pulse wave solution. The x-axis is spatial position; the y-axis is time with $t = 0$ at the top.

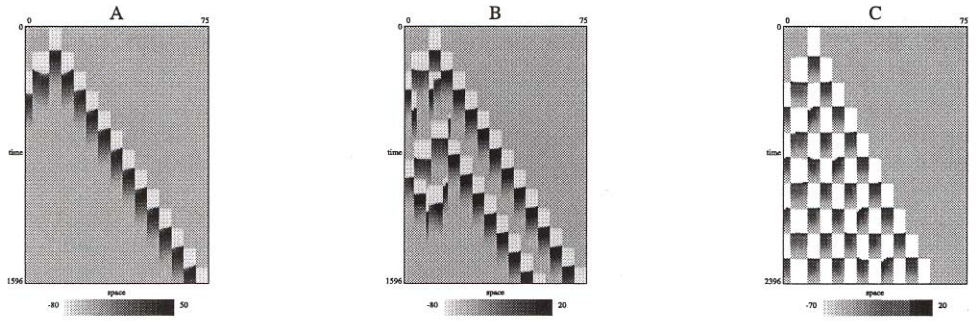

Figure 25: Lurching wave solutions found by simulation in [101]. Single- and multiple-pulse lurching wave solutions were found. In both cases the network returns to rest in the wake of the pulse. Sustained oscillation solutions were also found. These could be either synchronous oscillations or complex 'cluster' oscillations. (a) single-pulse solution; (b) multiple-pulse solution; (c) sustained cluster oscillation solution. The x-axis is spatial position; the y-axis is time with $t = 0$ at the top.

analytic estimation procedure for computing the expected velocity of smooth waves and the required size of the gap in the OFF-CENTER footprint required for smooth wave solutions.

Lurching wave solutions result from ON-CENTER synaptic footprints, although their analysis does not rule out the possibility that lurching waves might also be producible from OFF-CENTER footprints. Lurching waves involve clustered groups of neuronal activity, and their character is highly dependent upon the "wake" left behind the lurching wave. It was conjectured that each neuron in a cluster group fires synchronously with the others, and Terman et al. assumed that each neuron in a cluster group received the same amount of local inhibition. They provided conditions on the neural parameters required to ensure solitary wave (one-pulse) solutions. One condition found is that lurching waves cannot arise if the coupling constant g_{syn} is too small. They also obtained a result that lurching waves cannot arise in purely inhibitory networks. It should be noted that we do not at this time know whether or not lurching waves exist in the neocortex or elsewhere in biological systems.

The dynamics of this network are determined by the slow dynamics of the neurons and synaptic connections. This is in contrast to the usual situation in Fitzhugh-Nagumo-like dynamics where wave properties are determined by rapid processes. Also, in contrast to integrate-and-fire models and other models of excitation-driven waves, the slow-wave rather than the fast-wave solution is the stable one. (All the systems we have discussed have both slow-wave and fast-wave dynamics). [101] made no findings on the wave behavior of two-dimensional arrays of cells.

VIIC. Comparison of These Networks to Oscillator Networks. The networks just discussed have neuron-to-neuron couplings that are large enough to preclude using a phase-model approach, and the dynamics of the network coupling resembles FitzHugh-Nagumo coupling. Therefore the question arises as to why these networks do not seem to be bound to Wang's synchrony conjecture from section VI. The explanation here is simple. In contrast to section VI, where all the 'neurons' were oscillators with a characteristic eigenfrequency, the 'neurons' in section VII are not oscillators, do not have a characteristic eigenfrequency, and can fire at a number of different rates, including zero. As we have just observed above, periodic and even synchronous solutions *can* arise in these networks, but these solutions arise as a consequence of the large-scale network connectivity parameters and not because the 'neurons' themselves are oscillators.

The results reported in [101] underscore the importance of a role for local inhibition in a 'cluster netlet' of neurons. Although the Anninos model allowed for inhibitory connections, in that model these connections, like the excitatory ones, were made randomly. In sharp contrast, inhibitory connections in the neocortex are mostly local and however 'random' they may appear

within a local cluster, *globally* there is a great deal of non-random structure to inhibitory connections. This is something the Anninos model could not take into account. In the past several years it has come to be widely recognized that synchrony in spiking neuron networks can be – and biologically most likely is – greatly facilitated by the presence of local and lateral inhibitory connections among cells [102]-[104].

VIID. The Eckhorn Model. Of the network models we have so far examined, the one which seems to hold the most promise for explaining the experimental results reviewed earlier is the Terman et al. model of [102]. Unfortunately, however, signal propagation by post inhibitory rebound is not the main signaling mechanism in the neocortex. The success of these findings can at best be nothing more than a limited form of biological reality. In addition, the model of [102] is computationally somewhat expensive, and it is clear that a less expensive model is desirable. Over the years there have been a steady number of extensions and refinements starting from the simple LIF model. Gerstner and Kistler have developed a general class of neuron models that can be regarded as LIF generalizations; the family is called the spike response model (SRM) [81]. However, the arguably most popular present day model (after the LIF model) is one developed by Eckhorn et al., which we will here call the Eckhorn neuron [25].

The structure of the basic Eckhorn neuron and its schematic symbol is illustrated in figure 26.

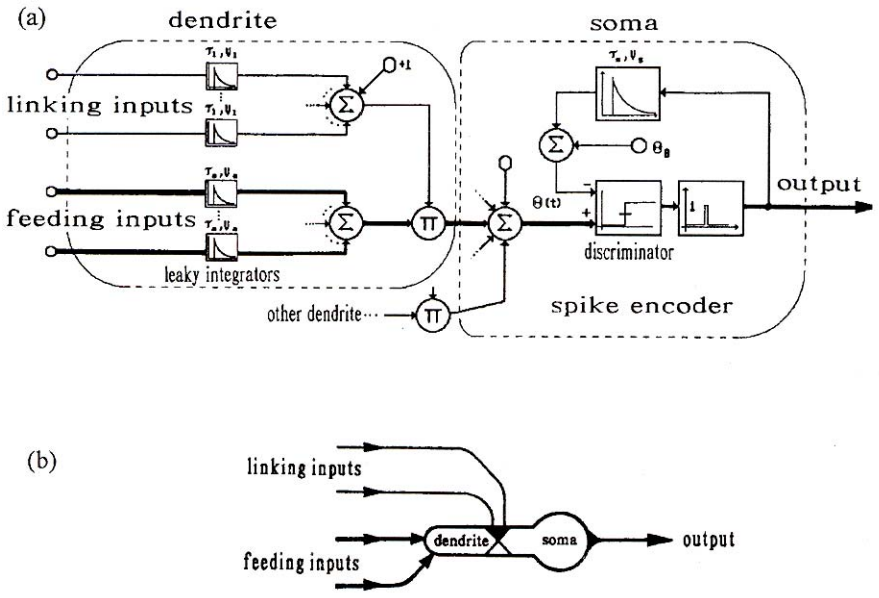

Figure 26: Basic Eckhorn neuron and its schematic symbol. It is a multicompartment model consisting of one pulse generator, called a neuromime, and one or more dendrites. Synaptic inputs are applied to the dendrite(s) and are of two types: feeding field inputs and linking field inputs.

The neuron is a multicompartment model consisting of a pulse-generating spike encoder ("soma") and one or more "dendrites." The spike encoder is often called a "neuromime." All synaptic inputs to the neuron are applied to the dendrite and are divided into two classes. Feeding field inputs are direct signal pathways and correspond to the classical excitatory or inhibitory ionotropic synaptic inputs (AMPA or $GABA_A$ receptors). No output pulse (action potential) can be stimulated from the neuron in the absence of feeding field inputs. Each input is weighted and integrated by a leaky integrator (LI) function. In principle both the weighting and the time constant of integration can differ for each feeding field input. In practice, most models assume the same time constant for each fielding field LI, which permits the neuron to be simplified by taking the integrators across the summing node shown in the figure and consolidating them all into a single LI at the output of the summing node. Letting Y_f represent the vector of feeding field input pulses and W_f denote the vector of feeding field synaptic weights (both vectors being column vectors), the summation of the feeding field inputs is $s_f = W_f^T Y_f$ and the feeding field response is given by a scalar state variable $x_f(t)$ according to the equation

$$\tau_f \frac{dx_f}{dt} = -x_f(t) + s_f(t) \tag{10}$$

where τ_f is the time constant of the feeding field LI.

The linking field inputs are the novel feature of the Eckhorn neuron. Like the feeding field inputs, each linking field input pulse is weighted and applied to a LI. Again, in practice the time constants of the linking field LIs are usually equal and so we can again use a single LI at the output of the summing node to process all the weighted linking field pulse inputs. Letting Y_l and W_l denote the vectors of the linking field inputs and synaptic weights, respectively, the summed linking field input is $s_l = W_l^T Y_l$ and the linking field response is represented by a scalar state variable x_l according to

$$\tau_l \frac{dx_l}{dt} = -x_l(t) + s_l(t) \tag{11}$$

where τ_l is the time constant of the linking field LI. Unlike the feeding field inputs, it is less clear what the linking field synapses correspond to in the biological neuron. The role of the linking field is to modulate the overall gain of the dendrite such that the dendrite output is

$$s_d(t) = x_f(t) \cdot [1 + x_l(t)] \quad . \tag{12}$$

In the absence of linking field inputs the dendrite output is given merely by its feeding field state variable. Note that the linking field cannot by itself produce an output s_d in the absence of feeding field excitation. If τ_l were much larger than τ_f the linking field synapses might be regarded as

metabotropic synapses [16], [17]. However, in practice τ_l is typically about an order of magnitude smaller than τ_f , which means the linking field dynamic response is very fast compared to the feeding field pathway. This is contrary to the character of metabotropic synaptic responses, which are typically an order of magnitude or more slower than ionotropic synaptic responses.

The Eckhorn soma models the summation and trigger response of a neuron's cell body. Unlike a biological neuron, where the soma typically has a large number of primarily inhibitory synaptic inputs, the Eckhorn soma has no synaptic inputs (although such inputs could be modeled by adding a separate 'inhibitory dendrite' either with or without linking field inputs). Its principal task is to implement a threshold-triggered AP response and to implement a refractory period after the firing of an AP. This is done through the use of a time-varying firing threshold $\theta(t)$. Let $d(t)$ denote the summation of all the dendritic outputs converging on the soma (left summing node in the spike encoder of figure 26). If at $t = 0$ we have $d(t) \geq \theta(t)$, the Eckhorn soma produces an output pulse

$$p(t) = \begin{cases} 1, & 0 < t < \tau_o \\ 0, & \text{otherwise} \end{cases} \tag{13}$$

where τ_o is the width of the action potential. The state of the soma is represented by a scalar state variable $x_n(t)$. Suppose the neuron generates its most recent action potential starting at time $t = t'$. Then

$$x_n(t) = \begin{cases} \theta_1, & 0 \leq t - t' < \tau_o \\ \theta_1 \cdot \exp\left(-\left(t - t' - \tau_o\right)/\tau_n\right), & t \geq t' + \tau_o \end{cases} \tag{14}$$

where τ_n is the time constant of the neuromime and θ_1 is a positive constant. Then

$$\theta(t) = \theta_o + x_n(t) \tag{15}$$

where θ_o is a positive constant that determines the minimum firing threshold of the neuromime. The neuron will not fire again until $\theta(t)$ decays back to equal $d(t)$. If $d > \theta_o$ is held constant, the next firing time for the neuron is given by

$$t'' = t' + \tau_o + \tau_n \ln\left(\frac{\theta_1}{d - \theta_o}\right) .$$

The interval between pulses for constant d is $\Delta T(d) = t'' - t'$, and so the firing rate for a constant input to the soma is

$$R(d) = \frac{1/\tau_o}{1 + \left(\tau_n/\tau_o\right) \cdot \ln\left(\theta_1/\left(d - \theta_o\right)\right)} .$$

VIIE. Eckhorn Neural Networks. The Eckhorn neuron model was originally developed as a model for synchronous firing activity observed in cat visual cortex [23]. Most Eckhorn networks

that have been studied and reported have been either one- or two-layer networks. A number of such networks are described in [37]. Figure 27 illustrates the most basic one-layer Eckhorn network. For clarity, connections between neurons are shown only for the cross-hatched neuron. All other neurons make topologically identical connections. Note that all these connections are applied to linking field inputs. The linking field vector W_l gives the synaptic 'footprint' for the coupling of the network. The receptive feeding field is defined by weight vector W_f . In some applications, only a scalar (one weight) feeding field input is applied to each neuron. When this is done it is often necessary to apply a small random 'noise' signal to the neuromime input (see figure 26). The 'noise' signal for each neuron should be statistically independent of the others. This is done so that the feeding field weight can be made small enough to avoid having the network display too much of a 'hair trigger' reaction to random feeding field inputs. The main purpose of the network configuration is to produce a synchronized vector of output pulses from some subset of neurons that 'encodes' the input feeding field pattern. Linking field weights are chosen so that the network as a whole 'filters out' the noise and produces an input-pattern-dependent response. When a stochastic 'noise' is not made part of the network, a scalar feeding field input usually has a synaptic weight set such that a high frequency burst of input pulses is required in order to trigger the neuron and a single random feeding field pulse cannot.

Two-layer Eckhorn networks are commonly encountered in applications related to image processing. They are capable of more complex input segmentation tasks. The generic two-layer Eckhorn network is illustrated in figure 28. Each individual layer is organized in the same way as in the one-layer network of figure 27. However, each layer-2 neuron typically receives feeding field inputs from several layer-1 neurons, and each layer-2 neuron provides linking field feedback

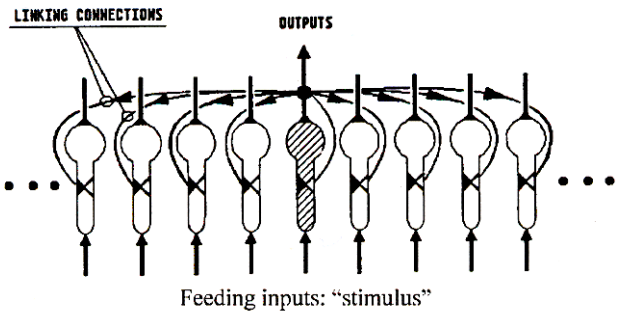

Figure 27: Basic one-layer Eckhorn network. Network coupling is by linking field connections only. The feeding field inputs may either be single input per neuron or vector inputs per neuron. Note that in the case of a single feeding field input either the synaptic weight of the feeding field must be large enough to trigger the neuron in response to a tetanus, but not a single pulse, or else some random 'noise' (not shown), must be added to each neuron. The feeding field weights for a single-input per neuron layers must be set so that the network is not too excitable or little useful signal processing results.

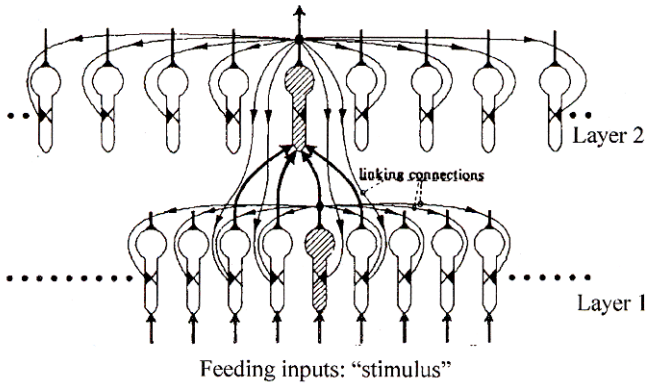

Figure 28: Typical two-layer Eckhorn neural network. Connections are shown only for the cross-hatched neurons. Each layer is similar to the single-layer configuration of figure 27 except that linking field connections feed back from each neuron in layer 2 to the neurons in layer 1 that provide feeding field inputs to that layer-2 neuron. The feeding field weight vector W_f of each layer-2 neuron defines its receptive field.

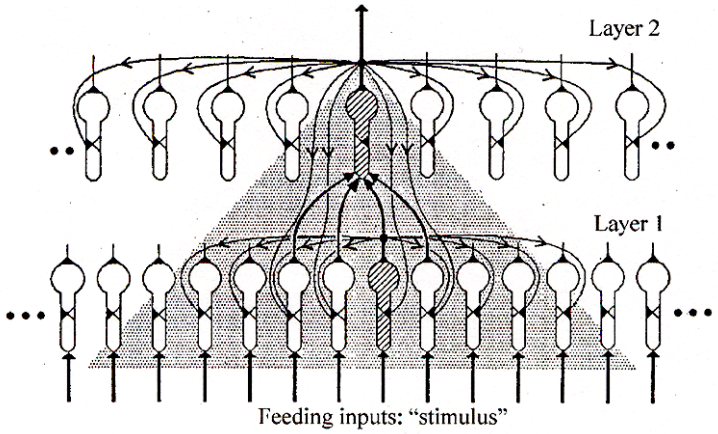

Figure 29: Contrast-enhancing Eckhorn network. The basic connections shown are the same as in figure 28. However, each layer-2 neuron also provides inhibitory feedback to the feeding field inputs to the layer-1 neurons in the shaded area. (The figure does not explicitly show this feedback). The inhibitory feedback footprint is an ON-CENTER footprint with a Gaussian decay in synaptic weights as the connection moves laterally away from the feedback center. The feeding field time constant for the inhibitory feedback is larger than the time constants for the feed-forward feeding field inputs. This implements a 'slow' feedback inhibition process that tends to suppress firing by neurons that are less synchronized, typically those at the edges of the cell group.

to each layer-1 neuron from which it receives a feeding field input. Traveling wave behavior across layer-2 outputs have been reported in image processing applications [105], although no formal theory has yet been presented to describe or explain this traveling wave activity.

Figure-background segmentation is an important capability in neural networks because such segmentation is regarded as necessary in order to permit multiple-object representation. Experiments in the visual cortex of the monkey suggest that encoding of segmentation takes place through temporal decorrelation due to different firing rates by different cell assemblies. (There is

no evidence that segmentation encoding takes place through phase shifts). The typical two-layer Eckhorn network of figure 28 produces synchronized firing by all participating layer-2 neurons. By adding inhibitory *feeding field* feedback from layer 2 to layer 1, it has been shown [37] that frequency-encoded figure-background contrast can be achieved. This is illustrated in figure 29. The inhibitory feedback employs a larger feeding field time constant than the feed-forward pathway into the feeding fields and therefore requires a separate LI for the inhibitory feeding field. This can be provided by adding an inhibitory 'dendrite', either with or without linking field.

Finally, Eckhorn networks that employ a common local inhibitory feedback to the linking field inputs can be used to 'chop up' synchronized firing patterns. The inhibitory feedback might also be applied to layer-1 feeding field inputs in some cases. This process is called rate-density modulation and it produces what Eckhorn has termed 'population spike packages.' This is illustrated in figure 30. The 'rate chopping' performed by this network is used to help partially synchronize firing patterns sent to downstream neurons and reduce transient activations in the local network.

VIII. Discussion

No formal methods for determining the various weights and time constants in Eckhorn networks have been reported, although some qualitative guidelines have been suggested [106]. It is also the

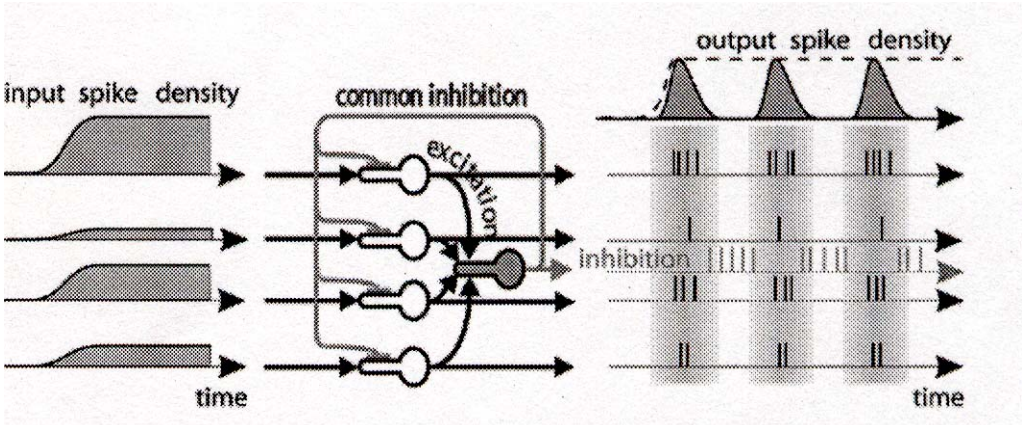

Figure 30: Rate-density modulation through local inhibitory feedback. Small local groups of layer-1 neurons provide excitatory feeding field inputs to a common inhibitory neuron in layer 2. Feedback from this neuron is commonly applied to the layer-1 neurons that feed it. The feedback may be to either the linking field inputs or to the layer-1 feeding field. The purpose of this configuration is to produced grouped 'packages' of layer-1 firing bursts as shown in the right-hand part of the figure. The left-hand graph denotes the density of incoming pulses, with higher density implying faster spiking rate. Note that the input spike density differs for the various layer-1 neurons. Layer-1 firing is suppressed by burst firing from the inhibitory interneuron. This generally requires a slow feeding field time constant for the inhibitory neuron in order to produce burst firing at its output. Lateral layer-1 connections are made as in figure 27 and are not shown in this figure.

case that Eckhorn networks have not received the sort of theoretical attention that has been provided by the mathematicians for coupled oscillator models or the network reported in [101]. No nullcline analysis has been made nor Lyapunov function developed for Eckhorn networks. Insight appears to have been the main design tool for coming up with network topologies, and one suspects trial-and-error has been the main tool for determining synaptic footprints and weights.

A criticism is sometimes leveled against LIF, Eckhorn, and the other neural network models we have reviewed. The criticism is that these networks are not composed of 'neurons' that produce the diversity of responses exhibited by real neurons (e.g. figures 4 – 9 and 13). It is argued that trustworthy theories of large-scale neural network behavior must look to Hodgkin-Huxley-like neuron models if the conclusions are to be held relevant to actual neurodynamics. The problem with network models based on Hodgkin-Huxley-like dynamics is one of computational complexity. The computational cost of simulating these networks is very high, and most researchers have therefore settled for less accurate but practically computable network models.

Recently there has been a breakthrough in large-scale Hodgkin-Huxley-like neural network modeling. **Rulkov** et al. introduced a phenomenological model, called the **map-based model**, that has been demonstrated to be capable of producing very Hodgkin-Huxley-like neurodynamics at a very low computational cost [107]. The first version of this model was reported by Rulkov in 2002 [108]. In this paper Rulkov provided a detailed phase-plane analysis describing how the different response modes of the model neuron come about and how the model parameters determine these in spiking and bursting modes. A follow up paper extended this analysis to a chaotic response region of the model [109]. The first application of this approach in a neural network was reported in [110]. The model was further extended in [107].

Although it is phenomenological, the model neurons are very low-cost-to-compute, having only two state variables (compared to three necessary for the Eckhorn neuron). Rulkov et al. reported simulating networks with more than $3 \cdot 10^5$ neurons (one of the largest simulations ever reported). They reported that a simulation with 6000 time-step iterations (roughly the equivalent of 3 seconds of neural activity) in a chain of 131,072 cells took just under 19 minutes on a workstation using a 1.4 GHz AMD Athlon processor with 512 Mbytes of memory running in Fortran 4.0 under a Windows 2000 operating system. Computation time was reported to scale linearly with network size. This is approximately 3 orders of magnitude faster than conventional Hodgkin-Huxley-like calculations. It was demonstrated in [107] that the Rulkov model did a credible job of producing RS-, FS-, and IB-like neural responses to stimuli, comparable to the

Wilson model results in this paper. The Rulkov model therefore definitely merits additional investigation and seems likely to become 'the' standard neuron model of the future.

Nonetheless, there is still a caution we must apply so as not to become over-enthusiastic about these exciting findings. Although the number of neurons that can be simulated with the Rulkov model is very large, it is still worthy of note that a functional column in the neocortex is comprised of tens of thousands of neurons with an average of 40,000 synaptic connections each [111]. The neural networks of Rulkov et al. did not contain anywhere near this number of synaptic connections. The number of presynaptic neurons converging on each RS-type cell in their network was on the order of 200. Therefore their two-dimensional network models are not to be regarded as actual models of the functional column organization of the neocortex. Models such as the Eckhorn network models, therefore, are not necessarily inferior to Rulkov models if we regard one- and two-layer Eckhorn networks as approximations of a functional column. The extensive local lateral connections in the Eckhorn network model are consistent with the cortical organization of figures 1 – 3 above, although the absence of lateral inhibition in the one-layer network is not. Still, it might be the case that an appropriately-configured two-layer Eckhorn neuron might be an adequate model for a functional column. One way to test this conjecture is to employ a very large number of Rulkov neurons connected up as suggested by the cortical circuit rules given earlier, and to then see if the cooperative behavior of a 'Rulkov column' and that of an appropriately-designed Eckhorn 'netlet' can be made similar. If a large Rulkov column can be adequately mimicked by a much smaller Eckhorn network, then a multi-scale approach to cortical modeling in which smaller Eckhorn netlets (or, for that matter, Rulkov netlets) can approximate a column defined by the properties of a larger Rulkov column mimic. This is a wide-open research question. Whether one would prefer 'Eckhorn columns' to a small-scale Rulkov 'column netlet' would ultimately depend on the relative network complexity of each, as measured in required computation time, and upon the following consideration.

One downside to functional column modeling using Eckhorn neurons is this. Eckhorn networks reported to date tend to fire synchronously at a single firing rate. This is not surprising because this is precisely the behavior Eckhorn et al. wanted to produce with this model. But, as we have seen, real neural networks display multi-frequency firing patterns (alpha- and beta- and gamma-band firing patterns). It is not presently known whether or not Eckhorn networks are capable of multi-synchronous multi-frequency firing pattern modes. Nor has it been reported if Eckhorn networks exhibit low-frequency 'membrane' fluctuations (*d* in the Eckhorn model) as shown above in figure 14. Equally, it has not been shown whether or not Rulkov netlets have this capability.

Neither necessary nor sufficient conditions for the production of either smooth waves or lurching waves in a large network of interconnected Eckhorn layers have been reported. This is probably owing to the absence of a formal mathematical treatment of Eckhorn neurodynamics and a natural consequence of researchers focusing their attention on gamma waves. It is known that wave behavior is observable in Eckhorn networks [105], but these waves have not been classified as either smooth or lurching waves. Self-propagating wave patterns have been demonstrated in large Rulkov networks [107]. Rulkov et al. have demonstrated that linear chains of Rulkov netlets can produce constant-velocity (smooth) waves. They have also discovered a mode of non-constant-velocity wave propagation under certain parametric conditions and have duplicated this in Hodgkin-Huxley networks. However, at present it seems to be the case that these non-constant-velocity waves are probably not lurching waves as reported in [101]. If the rough analysis stands up, these Rulkov waves will constitute yet a third class of wave propagation behavior in large-scale neural networks. Rulkov et al. have demonstrated that the qualitative character of propagating waves in a moderately large network changes as the size of the network is increased. Self-sustaining bifurcating spiral waves were found in a 128 × 128 Rulkov network. This bifurcating wave phenomenon was absent in an 80 × 80 network, which also did not self-sustain the wave activity. They reported that the critical size of the network needed to produce these self-sustaining waves depended on the footprint size of the synaptic connections. We therefore are faced with an interesting emergent property when the neural network size surpasses some critical point.

Yet another issue is that of understanding the wave mechanics of a complex neural network. It is one thing to obtain a network that displays interesting wave propagation properties. It is another to understand what sort of network is required to produce a *desired* wave property. It is only for the unrealistically simple phase and relaxation oscillator models discussed earlier where theoretical results that can be applied to the synthesis of a network have yet been obtained. Recently Hayon et al. have proposed an interesting approach to this issue in the case of synfire networks.

The basic ideas of a synfire chain and of coupled parallel synfire chains are illustrated in figure 31. Neurons are arranged in a column, called a **pool**. Each pool contains n neurons. Each neuron in a pool projects to $m \leq n$ neurons in the next pool in the chain. These are the intra-chain projections. In coupled synfire chains, each neuron makes $j << m$ projections to neurons in the parallel chain. All coupling is feedforward in the chain. A pool may contain inhibitory as well as excitatory neurons. With appropriate coupling, synfire chains can propagate synchronous activity waves. Here an activity wave is defined as a propagating pulse packet.

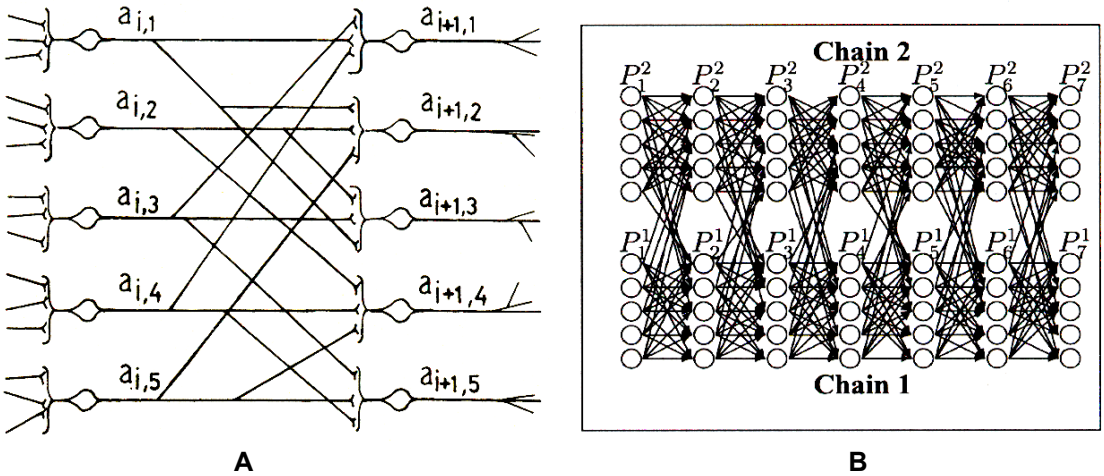

Figure 31: Synfire chain model. (A) Neuron pool. Each pool of neurons in a synfire chain contains n neurons, each of which makes $m \leq n$ projections to neurons in the next pool of the chain. (B) Linked parallel synfire chains. Each P column is a pool, and each pool projects to m neurons in the next link of its chain and also makes a much smaller number of projections to the adjacent parallel chains.

Abeles et al. have demonstrated that systems of interconnected synfire chains can synchronize their waves, and have studied various wave properties including velocity, time to synchronize, range of synchronization, bounds on the binding mechanisms between neurons in the same chain and between chains [112]. They also discussed mechanisms for getting systems of coupled synfire chains to segregate complex multi-object input stimuli through competition.

While these results were empirical rather than theoretical, their study of the behavior of these waves led to a follow-up work in which was presented a simpler approximate model of the observed wave mechanics [113]. In [112] it was found that even a relatively simple segregation-and-compositional binding problem required a very large number of neurons, on the order of $50 \cdot 10^3$ neurons, in the synfire network. However, in studying the observed wave behaviors they suggest that the wave action itself can be described using only wave position and velocity as the relevant variables. They obtained simple approximate expressions for various wave synchronization, creation, and extinction properties [113]. Inasmuch as there are rather obvious similarities between the synfire chain architecture and that of cascaded Eckhorn networks, it is a reasonable guess that their expressions, perhaps in some modified form, should apply to Eckhorn networks as well.

One weakness of the synfire model is its absence of local feedback connections. Such connections do exist within the functional columns of the neocortex (figures 1 through 3). Indeed, if a functional netlet is to be capable of generating multi-frequency waves, such local feedback connections would seem to be necessary. It follows from this observation that something like the Hayon ‘wave mechanics’ phenomenology could be extended to take in the case where the ‘pools’

have such local feedback. In this, the earlier findings of Eckhorn et al. would be highly relevant. Extending the Eckhorn findings to the case of neurons with a richer degree of neurodynamics, i.e. Eckhorn-like networks implemented with Rulkov neurons, is likewise a natural follow up. Furthermore, there is circumstantial experimental evidence that might point to the existence of parallel chain structures in the primary visual cortex. Bosking et al. have used optical techniques to study spatial coding of retinal position and stimulus orientation [114]. They found that the visual cortex possesses extraordinarily fine structure in the location of responding neurons coupled with a surprisingly consistent size to the responding areas. In looking at their images, it is not difficult to envision neuronal 'chains' comprised of 'pools' of interacting neurons.

One thing that is largely missing from most theoretical investigations such as those we have just cited is retroactive feedback, i.e. convergence zones. It seems clear from the simulations reported by Rulkov, Eckhorn, Abeles, and many others that activity waves do not necessarily propagate at the conduction velocity of the axons. It was mentioned earlier that gamma-band propagation at the very slow rate of 0.25 m/sec has been observed in monkey visual cortex. This has particular relevance for the Bruns-Eckhorn data [48] reviewed earlier. As mentioned before, the distance from electrodes in area A to electrodes in area B in this experiment was 40 to 80 mm. Assume for a moment that the gamma wave propagation was 0.25 m/sec, and further assume that retroactive feedback from area B to area A was in fact present, as illustrated in figure 32. At 40 mm distance, such a slow activity wave would require 160 msec to travel from A to B. Retroactive signaling would likewise require another 160 msec to return. The measured correlation lag in [48] was 40 msec, which as noted earlier appears to implicate polysynaptic coupling. If ELFS is an artifact of slow-wave coupling, it would seem possible that the correlation lag between stimulating a firing event (in B) and a responding low frequency signal

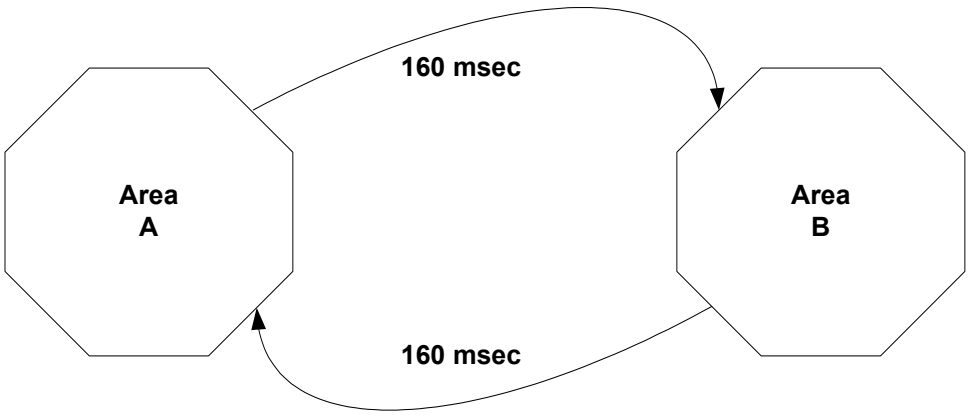

Figure 32: Hypothetical retroactive coupling at slow wave propagation velocities in the Bruns-Eckhorn experiment [48].

(in A) could require a lag time determined by the round trip time through the loop. A period of 320 msec corresponds to a frequency of 3.125 Hz, which places it within the low frequency range of [48]. The measurement data from [48] did not test beyond a ± 100 msec lag. We can further note that the dwell time for the measured correlations after activity plateau was 150 msec, a figure suspiciously in this ballpark. The bottom line of these observations is simply this: There might have been retroactive correlation (not necessarily in the gamma band) that simply went unobserved because it fell outside of the correlation measurement interval.

The study cited earlier tells us that in the case of asymmetric directional coupling the phenomenon of direction dominance in coupled chains must be recognized. However, this study involved only a single frequency. Does directional dominance exist when the coupling is asymmetric not only in coupling strength but in frequency as well? This is yet another open research question.

IX. Summary

In this paper we have reviewed various findings reported by both experimental and theoretical researchers. Our focus has been on contrasting and evaluating these findings in the context of known characteristics of the neocortex. Probably the most important question today in neuroscience is: How does the brain represent objects and events? The findings we have looked at are those which appear to be the most relevant for the hypothesis that the brain accomplishes its representation tasks through the mechanism of synchronized and/or correlated activity wave patterns. This is known as the **correlation hypothesis** of brain theory. However, in order to test this hypothesis it is necessary that we first understand the "wave mechanics" of neural network models that qualitatively resemble the measurable properties of activity waves observable in biological networks. Because it is a practical impossibility for us to construct neural network models that match biological networks neuron-for-neuron (owing to the incredible number of biological neurons in the central nervous system), we must settle for so-called "population models" that try to produce similar activity using far fewer neurons. However, even these models involve a great many "artificial neurons" or other more abstract "cells," a fact that makes it difficult and challenging to understand even our constructed artificial networks.

There is strong evidence of size-dependent emerging properties in the wave mechanics of large neural networks. This is yet another reason why network models involving large numbers of neuron models are necessary. So far these interesting emergent properties have only been seen in models based on Hodgkin-Huxley-like neuron models and in Rulkov neuron models. This tends to suggest that the rich dynamics of neural firing patterns might be necessary for the production

of these large-scale neurodynamics. So it is that developing a better understanding of the wave mechanics of these networks, both empirically and mathematically, is perhaps the fundamental research issue in present-day computational neuroscience.

References

1. David G. Amaral, "Anatomical organization of the central nervous system," in *Principles of Neural Science*, 4th ed., E.R. Kandel, J.H. Schwartz, and T.M. Jessell (eds.), NY: McGraw-Hill, 2000, pp. 317-336.

2. James P. Kelly, "The neural basis of perception and movement," in *Principles of Neural Science*, 3rd ed., E.R. Kandel, J.H. Schwartz, and T.M. Jessell (eds.), Norwalk, CN: Appleton & Lange, 1991, pp. 283-295. See especially pp. 292-293.

3. White, E.L., *Cortical Circuits: Synaptic Organization of the Cerebral Cortex, Structure, Function, and Theory*, Boston, MA: Birkhäuser, 1989.

4. H.R. Wilson (1999), "Simplified dynamics of human and mammalian neocortical neurons," *J. Theor. Biol.* **200,** 375-388.

5. Chagnac-Amitai, Y. and Connors, B.W. (1989), "Synchronized excitation and inhibition driven by intrinsically bursting neurons in neocortex," *J. Neurophysiol.* 62: 1149-1162.

6. H.R. Wilson, *Spikes Decisions and Actions: The Dynamical Foundations of Neuroscience*, Oxford, UK: Oxford University Press, 1999.

7. Shepherd, G.M. (1978), "Microcircuits in the nervous system," *Sci. Am.* 238: 92-103.

8. Gordon M. Shepherd, *Neurobiology*, 3rd ed., Oxford, UK: Oxford University Press, 1994.

9. Lucien Côté and Michael D. Crutcher, "The basal ganglia," in *Principles of Neural Science*, 3rd ed., E.R. Kandel, J.H. Schwartz, and T.M. Jessell (eds.), Norwalk, CN: Appleton & Lange, 1991, pp. 647-659.

10. Thomas P. Trappenberg, *Fundamentals of Computational Neuroscience*, Oxford, UK: Oxford University Press, 2002.

11. Toledo-Rodriguez, M., A. Gupta, Y. Wang, C.Z. Wu, and H. Markram, "Neocortex: Basic neuron types," in *Handbook of Brain Theory and Neural Networks*, 2nd ed., M.A. Arbib (ed.), pp. 719-725, Cambridge, MA: The MIT Press, 2003.

12. V. Braitenberg and A. Schüz, *Anatomy of the Cortex: Statistics and Geometry*, NY: Springer-Verlag, 1991.

13. Douglas, R. and K. Martin, "Neocortex," in *The Synaptic Organization of the Brain*, 4th ed., G.M. Shepherd (ed.), Oxford, UK: Oxford University Press, 1998, pp. 459-509.

14. Fairén, A., DeFelipe, J., and Regidor, J. (1984), "Nonpyramidal neurons: General account," in *The Cerebral Cortex*, Vol. 1, Cellular Components of the Cerebral Cortex, A. Peters and E.G. Jones (eds.), NY: Plenum Press, pp. 201-253.

15. Fleur L. Strand, *Neuropeptides: Regulators of Physiological Process*, Cambridge, MA: The MIT Press, 1999.

16. Siegelbaum, S.A., J.H. Schwartz, and E.R. Kandel, "Modulation of synaptic transmission: Second messengers," in *Principles of Neural Science*, 4th ed., E.R. Kandel, J.H. Schwartz, and T.M. Jessell (eds.), NY: McGraw-Hill, 2000, pp. 229-252.

17. Wells, R.B., "Modulation channels in biomimic artificial neurons," *Proc. 28th Ann. Conf. Indus. Electron. (IECON'02)*, Nov. 5-8, Sevilla, Spain, 2002, pp. 3209-3214.

18. Abeles, M., *Corticonics: Neural Circuits of the Cerebral Cortex*, Cambridge, UK: Cambridge University Press, 1991.

19. Schüz, A., "Neuroanatomy in a computational perspective," in *Handbook of Brain Theory and Neural Networks*, 2nd ed., M.A. Arbib (ed.), pp. 733-737, Cambridge, MA: The MIT Press, 2003.

20. Morris, C. and Lecar, H. (1981), "Voltage oscillations in the barnacle giant muscle fiber," *Biophys. J.* **35**: 193-213.

21. Terman, D.H., G.B. Ermentrout, and A.C. Yew, "Propagating activity patterns in thalamic neuronal networks," *SIAM J. Appl. Math.*, vol. 61, no. 5, pp. 1578-1604, 2001.

22. Von der Malsburg, C., "The correlation theory of brain function," in *Models of Neural Networks II: Temporal Aspects of Coding and Information Processing in Biological Systems*, E. Domany, J.L. van Hemmen, and K. Schulten (eds.), pp. 95-119, NY: Springer-Verlag, 1994.

23. Eckhorn, R., R. Bauer, W. Jordan, M. Brosch, W. Kruse, M. Munk, and H.J. Reitboeck, "Coherent oscillations: A method of feature linking in the visual cortex? multiple electrode and correlation analyzes in the cat," *Biol. Cybern.*, vol. 60, pp. 121-130, 1988.

24. Gray, C.M., P. König, A.K. Engel, and W. Singer, "Oscillatory responses in cat visual cortex exhibit inter-columnar synchronization which reflects global stimulus properties," *Nature*, vol. 338, pp. 334-337, 1989.

25. Eckhorn, R., H.J. Reitboeck, M. Arndt, and P. Dicke, "Feature linking via synchronization among distributed assemblies: Simulations of results from cat visual cortex," *Neural Computat.*, vol. 2, pp. 293-307, 1990.

26. Kreiter, A. and W. Singer, "Oscillatory neuronal responses in the visual cortex of the awake macaque monkey," *Eur. J. Neurosci.*, vol. 4, pp. 369-375, 1992.

27. Frien, A., R. Eckhorn, R. Bauer, T. Woelbern, and H. Kehr, "Stimulus-specific fast oscillations at zero phase between visual areas V1 and V2 of awake monkey," *Neuroreport*, vol. 5, pp. 2273-2277, 1994.

28. Damasio, A.R., "Time-locked multiregional retroactivation: A systems-level proposal for the neural substrate of recall and recognition," *Cognition* 33, pp. 25-62, 1989.

29. Damasio, A.R., "The brain binds entities and events by multiregional activation from convergence zones," *Neural Computat.*, vol. 1, pp. 123-132, 1989.

30. Fahle, M. and C. Koch, "Spatial displacements, but not temporal asynchrony, destroys figural binding," *Vis. Research*, vol. 35, pp. 491-494, 1995.

31. Ghose, G.M. and R.D. Freeman, "Oscillatory discharge in the visual system: Does it have a functional role?" *J. Neurophysiol.*, vol. 68, pp. 1558-1574, 1992.

32. Kiper, D.C., K.R. Gegenfurtner, and A. Movshon, "Cortical oscillatory responses do not affect vision segmentation," *Vis. Research*, vol. 36, pp. 539-544, 1996.

33. Leonards, U., W. Singer, and M. Fahle, "The influence of temporal phase differences on texture segmentation," *Vis. Research*, vol. 36, pp. 2689-2697, 1995.

34. Fries, P., P.R. Roelfsema, A.K. Engel, P. König, and W. Singer, "Synchronization of oscillatory responses in the visual cortex correlates with perception in interocular rivalry," *Proc. Nat. Acad. of Sci. USA*, vol. 94, pp. 12,699-12,704, 1997.

35. Kottmann, M. and R. Eckhorn, "Perception related synchronized oscillations in monkey striate cortex in a binocular rivalry task," *Soc. Neurosci. Abstract*, vol. 22, 255.10, 1996.

36. Kruse, W. and R. Eckhorn, "Inhibition of sustained gamma oscillations by fast transient responses in cat visual cortex," *Proc. Nat. Acad. of Sci. USA*, vol. 93, pp. 6112-6117, 1996.

37. Eckhorn, R., "Neural mechanisms of visual feature binding investigated with microelectrodes and models," *Visual Cognition*, vol. 6 (3/4), pp. 231-265, 1999.

38. Damasio, A.R., *Descartes' Error*, NY: Avon Books, 1994.

39. Damasio, A.R., *The Feeling of What Happens*, NY: Harcourt, Brace & Co., 1999.

40. Damasio, A.R., T.J. Grabowski, A. Bechara, H. Damasio, L.L.B. Ponto, J. Parvizi, and R.D. Hichwa, "Subcortical and cortical brain activity during the feeling of self-generated emotions," *Nature Neurosci.*, vol. 3, no. 10, pp. 1049-1056, 2000.

41. Bechara, A., H. Damasio, and A.R. Damasio, "Emotion, decision making and the orbito-frontal cortex," *Cere. Cortex.*, vol. 10, pp. 295-307, 2000.

42. Lösel, F. and M. Schmucker, "Psychopathy, risk taking, and attention: a differentiated test of the somatic marker hypothesis," *J. Abn. Psych.*, vol. 113, no. 4, pp. 522-529, 2004.

43. Burgess, P.W., S.K. Scott, and C.D. Firth, "The role of the rostral frontal cortex (area 10) in prospective memory: a lateral versus medial dissociation," *Neuropsychologia*, vol. 41, pp. 906-918, 2003.

44. Eckhorn, R., A. Frien, R. Bauer, T. Woelbern, H. Kehr, "High frequency (30-90 Hz) oscillations in primary visual cortex of awake monkey," *Neuroreport*, vol. 4, pp. 243-246, 1993.

45. Gabriel, A. and R. Eckhorn, "A multi-channel correlation method detects traveling γ-waves in monkey visual cortex," *J. Neurosci. Methods*, vol. 131, pp. 171-184, 2003.

46. Bruns, A., R. Eckhorn, H. Jokeit, and A. Ebner, "Amplitude envelope correlation detects coupling among incoherent brain signals," *Neuroreport*, vol. 11, pp. 1509-1514, 2000.

47. Frien, A. and R. Eckhorn, "Functional coupling shows stronger stimulus dependency for fast oscillations than for low-frequency components in striate cortex of awake monkey," *Eur. J. Neurosci.*, vol. 12, pp. 1466-1478, 2000.

48. Bruns, A. and R. Eckhorn, "Task-related coupling from high- to low-frequency signals among visual cortical areas in human subdural recordings," *Int. J. Psychophysiol.*, vol. 51, pp. 97-116, 2004.

49. Kleinfeld, D., Delaney, K.R., Fee, M.S., Flores, J.A., Tank, D.W., and Gelperin, A., "Dynamics of propagating waves in the olfactory network of a terrestrial mollusk: An electrical and optical study," *J. Neurophysiol.*, vol. 72, pp. 1402-1419, 1994.

50. Prechtl, J.C., Bullock, T.H., and Kleinfeld, D., "Direct evidence for local oscillatory current sources and intracortical phase gradients in turtle visual cortex," *Proc. Nat. Ac. Sci. USA*, vol. 97, pp. 877-882, 2000.

51. Freeman, W.J. and Barrie, J.M., "Analysis of spatial patterns of phase in neocortical gamma EEGs in rabbit," *J. Neurophysiol.*, vol. 84, pp. 1266-1278, 2000.

52. Ribary, U., Ioannides, A., Singh, K., Hasson, R., Bolton, J., et al., "Magnetic field tomography of coherent thalamocortical 40 Hz oscillations in humans," *Proc. Nat. Ac. Sci. USA*, vol. 88, pp. 11037-11041, 1991.

53. Golomb, D. and Amitai, Y., "Propagating neuronal discharges in neocortical slices:

Computational and experimental study," *J. Neurophysiol.*, vol. 78, pp. 1199-1211, 1997.

54. Wadman, W.J. and Gutnick, M.J., "Non-uniform propagation of epileptiform discharge in brain slices of rat neocortex," *Neurosci.*, vol. 52, pp. 255-262, 1993.

55. Bringuier, V., Chavane, F., Glaeser, L., and Fregnac, Y., "Horizontal propagation of visual activity in the synaptic integration field of area 17 neurons," *Science*, vol. 283, pp. 695-699, 1999.

56. Volgushev, M., J. Pernberg, and U.T. Eysel, "A novel mechanism of response selectivity of neurons in cat visual cortex," *J. Physiol.*, vol. 540.1, pp. 307-320, 2002.

57. Anderson, J., H. Lampl, I. Reichova, M. Carandini, and D. Ferster, "Stimulus dependence of two-state fluctuations of membrane potential in cat visual cortex," *Nat. Neurosci.*, vol. 3, no. 6, pp. 617-621, June, 2000.

58. Eckhorn, R., A.M. Gail, A. Bruns, A. Gabriel, B. Al-Shaikhli, and M. Saam, "Different types of signal coupling in the visual cortex related to neural mechanisms of associative processing and perception," *IEEE Tr. Neural Networks*, vol. 15, no. 5, Sept. 2004, pp. 1039-1052.

59. Bullock, T.H., McClune, M.C., Achimowicz, I.Z., Iragui-Madoz, V.J., Duckrow, R.B. and Spencer, S.S., "EEG coherence has structure in the millimeter domain: Subdural and hippocampal recordings from epileptic patients," *Electroencephalogr. Clin. Neurophysiol.*, vol. 95, pp. 161-177, 1995.

60. Menon, V. Freeman, W.J., Cutillo, B.A. Desmond, J.E., Ward, M.F., et al., "Spatio-temporal correlations in human gamma band electrocorticograms," *Electroencephalogr. Clin. Neurophysiol.*, vol. 98, pp. 89-102, 1996.

61. Gross, D.W. and Gotman, J., "Correlation of high-frequency oscillations with the sleep-wake cycle and cognitive activity in humans," *Neurosci.*, vol. 94, pp. 1005-1018, 1999.

62. Bishop, G.H. and J.M. Smith, "The size of nerve fibers supplying the cerebral cortex," *Exp. Neurol.*, vol. 9, pp. 483-501, 1964.

63. Haug, H., M. Kelln, and A. Rost, "The postnatal development of myelinated nerve fibers in the visual cortex of the cat," *Cell Tissue Res.*, vol. 167, pp. 265-268, 1976.

64. Martin, J.H. and Jessell, T.M., "Modality coding in the somatic sensory system," in *Principles of Neural Science*, 3rd ed., E.R. Kandel, J.H. Schwartz, and T.M. Jessell (eds.), Norwalk, CN: Appleton & Lange, 1991, pp. 341-352.

65. Kuramoto, Y., "Self-entrainment of a population of coupled nonlinear oscillators," in *International Symposium on Mathematical Problems in Theoretical Physics*, H. Araki (ed.), Berlin: Springer-Verlag, 1975, pp. 420-422.

66. Kuramoto, Y., "Cooperative dynamics of oscillator community," *Progr. Theor. Phys. Suppl.*, vol. 79, pp. 223-240, 1984.

67. Kuramoto, Y., *Chemical Oscillations, Waves, and Turbulence*, Berlin: Springer-Verlag, 1984, pp. 68-77.

68. Kuramoto, Y., "Statistical macrodynamics of large dynamical systems. Case of a phase transition in oscillator communities," *J. Stat. Phys.*, vol. 49, pp. 569-605, 1987.

69. Gerstner, W. and J. Leo van Hemmen, "Coding and information processing in neural networks," in *Models of Neural Networks II: Temporal Aspects of Coding and Information Processing in Biological Systems*, E. Domany, J.L. van Hemmen, and K. Schulten (eds.), pp. 1-93, NY: Springer-Verlag, 1994.

70. Schuster, H.G. and Wagner, P., "A model of neuronal oscillations in the visual cortex: 2.

Phase description and feature dependent synchronization," *Biol. Cybern.*, vol. 64, pp. 77-82, 1990.

71. Wang, D.L., "Emergent synchrony in locally coupled neural oscillators," *IEEE Tr. Neural Netw.*, vol. 6, no. 4, pp. 941-948, 1995.

72. Wilson, H.R. and J.D. Cowan, "Excitatory and inhibitory interactions in localized populations of model neurons," *Biophys. J.*, vol. 12, pp. 1-24, 1972.

73. Von der Malsburg, C., "The what and why of binding: The modeler's perspective," *Neuron*, vol. 24, pp. 95-104, Sept., 1999.

74. Von der Malsburg, C. and W. Schneider, "A neural cocktail-party processor," *Biol. Cybern.* 54, pp. 29-40, 1986.

75. Von der Malsburg, C., "Dynamic link architecture," in *Handbook of Brain Theory and Neural Networks*, 2nd ed., M.A. Arbib (ed.), pp. 365-368, Cambridge, MA: The MIT Press, 2003.

76. Hodgkin, A.L. and Huxley, A.F., "A quantitative description of membrane current and its application to conduction and excitation in nerve," *J. Physiol. Lond.*, vol. 117, pp. 500-544, 1952.

77. Huguenard, J.R. and McCormick, D.A., "Simulation of the currents involved in rhythmic oscillations in thalamic relay neurons," *J. Neurophysiol.*, vol. 68, no. 4, pp. 1373-1383, 1992.

78. Huguenard, J.R. and McCormick, D.A., "A model of the electrophysiological properties of thalamocortical relay neurons," *J. Neurophysiol.*, vol. 68, no. 4, pp. 1384-1400, 1992.

79. Wilson, C.J. and Callaway, J.C., "Coupled oscillator model of dopaminergic neuron of the substantia nigra," *J. Neurophysiol.*, vol. 83, pp. 3084-3100, 2000.

80. FitzHugh, R., "Impulses and physiological states in theoretical models of nerve membranes," *Biophys. J.*, vol. 1, pp. 445-466, 1961.

81. Wulfram Gerstner and Werner Kistler, *Spiking Neuron Models*, Cambridge, UK: Cambridge University Press, 2002.

82. Terman, D. and W.L. Wang, "Global competition and local cooperation in a network of neural oscillators," *Physica D*, vol. 81, pp. 148-176, 1995.

83. Campbell, S.R., D.-L. Wang, and C. Jayaprakash, "Synchronization rates in classes of relaxation oscillators," *IEEE Tr. Neural Networks*, vol. 15, no. 5, Sept. 2004, pp. 1027-1038.

84. Campbell, S.R., D.L. Wang, and C. Jayaprakash, "Synchrony and desynchrony in integrate-and-fire neurons," *Neural Computat.*, vol. 7, pp. 1595-1619, 1999.

85. S.R. Campbell, *Synchrony and Desynchrony in Neural Oscillators*, Ph.D. Dissert., Dept. Phys. The Ohio State University, Columbus, OH, 1997.

86. Medvedev, G. and N. Kopell, "Synchronization and transient dynamics in chains of FitzHugh-Nagumo oscillators using strong electrical coupling," *SIAM J. Appl. Math.*, vol. 61, pp. 1762-1801, 2001.

87. Kopell, N. and G.B. Ermentrout, "Chains of oscillators in motor and sensory systems," in *Handbook of Brain Theory and Neural Networks*, 2nd ed., M.A. Arbib (ed.), Cambridge, MA: The MIT Press, 2003, pp. 201-205.

88. Cohen, A.H, Holmes, P.J., and Rand, R.H., "The nature of the coupling between segmental oscillators in the lamprey spinal generator for locomotion: A mathematical model," *J. Math. Biol.*, vol. 13, pp. 345-369, 1982.

89. Cohen, A., Ermentrout, G.B., Kiemel, T., Kopell, N., Sigvardt, K., and Williams, T.,

"Modeling of intersegmental coordination in the lamprey central pattern generator for locomotion," *Trends in Neurosci.*, vol. 15, pp. 434-438, 1992.

90. Ermentrout, G.B. and N. Kopell, "Inhibition-produced patterning in chains of coupled nonlinear oscillators," *SIAM J. Appl. Math.*, vol. 54, pp. 478-507, 1994.

91. Ermentrout, G.B. and Kopell, N., "Parabolic bursting in an excitable system coupled with a slow oscillation," *SIAM J. Appl. Math.*, vol. 15, pp. 215-237, 1986.

92. Chris Eliasmith and Charles H. Anderson, *Neural Engineering*, Cambridge, MA: The MIT Press, 2003.

93. Bressloff, P.C., "Synaptically generated wave patterns in excitable neural media," *Phys. Rev. Lett.*, vol. 82, pp. 2979-2982, 1999.

94. Ermentrout, G.B., "The analysis of synaptically generated traveling waves," *J. Comp. Neurosci.*, vol. 5, pp. 191-208, 1998.

95. Osan, R., J. Rubin, and B. Ermentrout, "Regular traveling waves in a one-dimensional network of theta neurons," *SIAM J. Appl. Math.*, vol. 62, no. 4, pp. 1197-1221, 2002.

96. Anninos, P.A., B. Beek, T.J. Csermely, E.M. Harth, and G. Pertile, "Dynamics of neural structures," *J. Theor. Biol.*, vol. 26, pp. 121-148, 1970.

97. Pantiliat, S., *Theoretical Model of the Nervous System*, Ph.D. dissert., The Hebrew University, Jerusalem, 1985.

98. Nelken, I., *Analysis of a Single Neuron in a Random Net*, M.Sc. thesis, The Hebrew University, Jerusalem, 1985.

99. Nelken, I., "Analysis of the activity of single neurons in stochastic settings," *Biol. Cybern.*, vol. 59, pp. 201-215, 1988.

100. Rinzel, J., D. Terman, X.-J. Wang, and B. Ermentrout, "Propagating activity patterns in large-scale inhibitory neuronal networks," *Science*, vol. 279, pp. 1351-1355, 1998.

101. Terman, D.H., G.B. Ermentrout, and A.C. Yew, "Propagating activity patterns in thalamic neuronal networks," *SIAM J. Appl. Math.*, vol. 61, no. 5, pp. 1578-1604, 2001.

102. Van Vreeswijk, C., L.F. Abbott, and G.B. Ermentrout, "When inhibition not excitation synchronizes neural firing," *J. Comput. Neurosci.*, vol. 1, pp. 313-321, 1994.

103. Freeman, W.J., "Feedback models of gamma rhythms," *Trends Neurosci.*, vol. 19, pp. 468-470, 1996.

104. Bush, P. and T.J. Sejnowski, "Inhibition synchronizes sparsely connected cortical neurons within and between columns in realistic network models," *J. Comput. Neurosci.*, vol. 3, pp. 91-110, 1996.

105. Johnson, J.L. and D. Ritter, "Observation of periodic waves in a pulse-coupled neural network," *Optics Letters*, vol. 18, no. 15, pp. 1253-1255, Aug. 1, 1993.

106. J.L. Johnson, Pulse-coupled neural nets: translation, rotation, scale, distortion, and intensity signal invariance for images, *Applied Optics*, vol. 33, no. 26, 10 Sept., 1994, pp. 6239-6253.

107. Rulkov, N.F., Timofeev, I., and Bazhenov, M., "Oscillations in large-scale cortical networks: Map-based model," *J. Computat. Neurosci.*, vol. 17, pp. 203-223, 2004.

108. Rulkov, N.F., "Modeling of spiking-bursting neural behavior using two-dimensional maps," *Phys. Rev. E, Stat. Nonlin. Soft Matter Phys.*, vol. 65, 041922, 2002.

109. Shilnikov, A.L. and Rulkov, N.F., "Origin of chaos in a two-dimensional map modeling spike-bursting neural activity," *Int. J. Bif. and Chaos*, vol. 13, no. 11, pp. 3325-3340, 2003.

110. Bazhenov, M., Timofeev, I., Steriade, M., Sejnowski, T.J., "Model of thalamocortical slow-wave sleep oscillations and transitions to activated states," *J. Neurosci.*, vol. 22, pp. 8691-8704, 2002.

111. Schütz, A., "Neuroanatomy in a computational perspective," in *Handbook of Brain Theory and Neural Networks*, 2nd ed., M.A. Arbib (ed.), pp. 733-737, Cambridge, MA: The MIT Press, 2003.

112. Abeles, M., Hayon, G., and Lehmann, D., "Modeling compositionality by dynamic binding of synfire chains," *J. Computat. Neurosci.*, vol. 17, pp. 179-201, 2004.

113. Hayon, G., Abeles, M., and Lehmann, D., "A model for representing the dynamics of a system of synfire chains," *J. Computat. Neurosci.*, vol. 18, pp. 41-53, 2005.

114. Bosking, W.H., J.C. Crowley and D. Fitzpatrick, "Spatial coding of position and orientation in primary visual cortex," *Nature Neurosci*., vol. 5, no. 9, pp. 874-882, Sept., 2002.